Supporting Information

for

High-frequency and -field EPR (HFEPR) Investigation of a Pseudotetrahedral Cr^{IV} Siloxide Complex and Computational Studies of Related $Cr^{IV}L_4$ Systems

Lukas Bucinsky,[€] Martin Breza,[€] Michal Malček, [€] David C. Powers,[▼] Seung Jun Hwang,[†] J. Krzystek,[$] Daniel G. Nocera,[†] and Joshua Telser[l,]*

[€] Institute of Physical Chemistry and Chemical Physics, of Chemical and Food Technology, Slovak University of Technology, Radlinského 9, SK-81237 Bratislava, Slovakia.
[▼] Department of Chemistry, Texas A&M University, College Station, Texas 77843, United States.
[†] Department of Chemistry and Chemical Biology, Harvard University, 12 Oxford Street, Cambridge, Massachusetts 02138, United States.
[$] National High Magnetic Field Laboratory, Florida State University, Tallahassee, Florida 32310. United States.
[l] Department of Biological, Chemical and Physical Sciences, Roosevelt University, Chicago, Illinois 60605, United States.

Table of Contents

I. Extended discussion of EPR in the context of ML_4 complexes where M = d^2 ion.

a) Conventional EPR of $S = 1$ complexes

Molecular complexes of general formula $Cr^{IV}L_4$, such as where L = R = 1-norbornyl,[1] $CH_2CMe_nPh_{3-n}$ (n = 0 – 3),),[2-4] L = $Ar^{n}Cl$ = pentachlorophenyl, 2,4,6-trichloro-phenyl, and 2,6-dichlorophenyl,[5-6] and L = OR = O^{t}Bu anions.[7] have been investigated by X-band EPR. In these nearly tetrahedral complexes (see Tables S1 and S2), the zfs is very small (D = 0 for a perfectly tetrahedral d^2 complex; see section II below) so that the EPR signal is often superficially similar to that of a spin doublet, namely an isotropic $\Delta M_S = \pm 1$ transition at a g value slightly below 2.0, as expected for a less than half-filled electron shell. There is in addition, a weak feature at low magnetic field, a so-called "half-field transition", or B_{min}, which is a signature of triplet EPR response and corresponds to a turning point in the $\Delta M_S = 2$ transition ($\langle S, M_S| = \langle 1, \pm 1| \rightarrow \langle 1, \mp 1|$). Also, a feature near g = 2.0, but sharper than the $\Delta M_S = \pm 1$ transition may appear, which is due to a double-quantum (DQ) transition ($\langle S, M_S| = \langle 1, \pm 1| \rightarrow \langle 1, 0| \rightarrow \langle 1, \mp 1|$). The DQ transition has been studied in the case of Ni^{II} complexes,[8] which are relevant here since octahedral d^8 is equivalent to tetrahedral d^2, by the electron-hole formalism. Altogether, this type of EPR spectrum is not particularly informative, except to demonstrate that the ground state is indeed a triplet with very small zfs ($|D| \ll h\nu$). In contrast, frozen solution X-band EPR spectra of several tetraalkylchromium(IV) complexes,[3] exhibited a triplet pattern,[9-10] with resolved fine structure, so that zfs parameters could be directly extracted. These results inspired us to calculate the zfs for such complexes by modern computational methods. Conventional EPR had also been applied to analogous tetraamidochromium species, but no signals were observed. The explanation proposed was that the minimum temperature employed (98 K) was too high and that liquid helium temperatures would have been required.[11] However, given that

tetraalkylchromium(IV) complexes gave EPR spectra even at room temperature,[4] and in frozen solution at 140 K,[3] the failure to observe spectra from $Cr(NR_2)_4$ at even lower temperatures suggests that temperature may not have been the problem. Moreover, we observed HFEPR spectra for $Cr(DTBMS)_4$ at temperatures as high as 282 K. Instead, it may be that the zfs of $Cr(NR_2)_4$ complexes is too large for observation at conventional frequencies and fields. Although such amido complexes have yet to be structurally characterized and thus is beyond the scope of this study, $Cr(NR_2)_4$ was subject to computational analysis to shed light on previous experimental studies and to provide insight into the electronic structure of a range of homoleptic CrL_4 species.

Lastly, we note that isoelectronic, spin triplet V^{III} complexes, $[V(Ar^{nCl})_4]^-$ afforded X-band EPR spectra from which zfs parameters were determined.[12-13] In the sole structurally characterized complex, $[V(C_6Cl_5)_4](NEt_4)$ (CSD code OCEWIC), the perchlorophenyl groups lead to a relatively larger deviation from tetrahedral geometry than in any of the CrL_4 complexes, whether from XRD or calculated geometries (see Table S1). Analysis of X- and Q-band spectra afforded the following spin Hamiltonian parameters: $|D| = 0.453$ cm^{-1}, $|E| = 0.72$ cm^{-1} ($|E/D| = 0.16$), $g = 1.98$. [12] These values are comparable to those observed for $Cr(DTBMS)_4$ and show the effect of the bulky and non-cylindrical perchlorophenyl ligands. Computational analysis of these V^{III} complexes is beyond the scope of this study.

b) Heterogeneity in EPR spectra of $S = 1$ ML_4 complexes

The modest spin Hamiltonian parameter differences among the three spin triplet species observed (A, B, and C) for $Cr(DTBMS)_4$, and their temperature dependence, may be related to disorder in the solid material. The published crystal structure shows disorder in the *t*-Bu groups of DTBMS.[14] Small structural changes, which could also be temperature dependent, can affect

the zero-field splitting of high-spin complexes, such as has been documented for Mn^{III}[15] and V^{III}.[16-17]

Similar heterogeneity was observed by Mowat et al. for the complexes CrR_4 (R = CH_2CMe_3, CH_2SiMe_3, and CH_2CMe_2Ph), even in frozen solution.[3] There would have been no reason for these workers to study their complexes in the solid state, given their solubility in non-coordinating solvents and the sensitivity of X-band EPR to nearly isotropic species with $g \approx 2.0$. For example, in petroleum ether (a non-interacting solvent) $Cr(CH_2SiMe_3)_4$ clearly gave two distinct spin triplet species as seen by X-band EPR at 115 K. This heterogeneity was extensively discussed by Mowat et al. and they concluded that it was due to different molecular conformations, perhaps due to rotation about the Cr-C bond. Other tetraalkylchromium(IV) complexes exhibited heterogeneity in their frozen solution X-band EPR spectra, but distinct triplet species could not be identified.[3] Likewise, Ward et al. observed four species for $Cr(Nor)_4$ in frozen isooctane solution at 93 K (zfs parameters are given in Table 4, main text).[1] Due to the microwave frequency in HFEPR being one, or possibly nearly two, orders of magnitude larger than the X-band microwave quantum (~100 GHz ≤ ν < 900 GHz versus ~9 GHz ≤ ν < 10 GHz, respectively), with a corresponding larger magnetic field range, the spectral resolution of HFEPR is much greater. Thus, the three similar triplet species in $Cr(DTBMS)_4$ were easily resolved, and HFEPR might also resolve distinct CrR_4 triplet species as well.

II. Extended discussion of LFT as applied to CrL_4 complexes.

a) Discussion of electronic spectra of CrR_4 complexes, R = Me, CH_2CMe_3, CH_2SiMe_3, Nor.

Each of the CrR_4 complexes reported by Mowat *et al*. exhibited a strong ($\varepsilon \approx 1000$ L mol^{-1} cm^{-1}) band observed at ~20 000 cm^{-1} (~500 nm), which was thus assigned to $^3A_2 \rightarrow {}^3T_1(F)$.[3] Fixing the Racah parameter somewhat arbitrarily to B = 450 cm^{-1} with

assignment of this band to $^3A_2 \rightarrow {}^3T_1(F)$ yields only slight variation among the σ-bonding parameters in T_d symmetry: R = Me: ε_σ = 12 996 cm^{-1}; CH_2CMe_3: ε_σ = 12 202.5 cm^{-1}; CH_2SiMe_3: ε_σ = 10 986 cm^{-1}.

The more recent, detailed study by Abrahamson *et al.* identified in $Cr(Nor)_4$, in addition to the main band at 20 580 cm^{-1} (486 nm, ε = 1340), a second transition at 16 130 cm^{-1} (620 nm), which was assigned to $^3A_2 \rightarrow 3T_2$.[18,19] Using these two transitions, a unique solution to the LFT parameters for a CrR_4 species with T_d point group symmetry obtains, namely Racah B = 409.870(5) cm^{-1} (~40% of the free-ion value;[20] possible in such a covalent complex) and either the crystal-field[21] parameter Dq = 1613.0 cm^{-1} or the angular overlap model (AOM)[22] parameter ε_σ = 12097.5 cm^{-1}, where $\left(\varepsilon_\sigma = \left(\frac{15}{2}\right) Dq\right)$. The transition $^3A_2 \rightarrow {}^3T_1(P)$ is calculated to be at 33 958 cm^{-1} (294 nm), which, perhaps coincidentally, agrees exactly with a shoulder observed on a strong ligand-to-metal charge-transfer (LMCT) band.[18] Use of Racah C/B = 4.11, C = 1684.6 cm^{-1},[20] gives spin forbidden (i.e., spin-flip within $e^2t_2^0$) transitions $^3A_2 \rightarrow {}^1E$ and $^1A_1$ at respectively 6587 and 12 247 cm^{-1} (see Table S3, for the AOM parameters for $Cr(Nor)_4$ and other CrL_4 complexes), neither of which corresponds to the shoulders reported at 18 730 cm^{-1} (534 nm) and 18 080 cm^{-1} (553 nm).[18]

Using the analysis for $Cr(Nor)_4$,[18] we return to the work of Mowat et al.,[3] who did report two components for each of the visible bands, as follows: $CrMe_4$ (20 000 cm^{-1} and 22 200 cm^{-1} (ε ≈ 600)), $Cr(CH_2CMe_3)_4$ (18 500 cm^{-1} and 21 100 cm^{-1} (ε = 1090)), and $Cr(CH_2SiMe_3)_4$ (17 100 cm^{-1} and 19 400 cm^{-1} (ε = 1060)). In the case of $CrMe_4$ the bands are too close together to be used viably, but for $Cr(CH_2CMe_3)_4$ and $Cr(CH_2SiMe_3)_4$, it is possible to fit exactly the

assignment of the observed bands, respectively with ε_σ = 13 875.0 cm^{-1} and 12 825.0 cm^{-1}, but with an unreasonably low Racah *B* parameter; respectively, 225.9 cm^{-1} and 199.4 cm^{-1} – only ~20% of the free-ion value. Therefore, the two components instead represent a tetragonal splitting, which also gives rise to the small zfs observed in X-band EPR, but absent structural information, is not worth pursuing. Mowat et al. also observed a very weak band at ~15 000 cm^{-1}, which may indeed be from $^3A_2 \rightarrow {}^3T_2$. Such an assignment gives ε_σ = 11 250 cm^{-1} for $Cr(CH_2CMe_3)_4$ and $Cr(CH_2SiMe_3)_4$, respectively with *B* = 613.4 cm^{-1} and 409.1 cm^{-1}. As noted by Mowat et al.,[3] $^3A_2 \rightarrow {}^3T_2$ should be very sensitive to the donor strength of the ligands, so use of the same, approximate value for both complexes is useful only in giving a rough idea as to the electronic structure of the complexes. Nevertheless, simple LFT adequately explains the key electronic spectral features of a range of tetraalkylchromium(IV) complexes.

Inclusion of spin-orbit coupling (SOC), e.g., with ζ = 180 cm^{-1} (~60% of the free-ion value[23]), only minimally affects the transitions and thus does not provide an explanation for the observed shoulders at ~18 500 cm^{-1} (~540 nm). SOC does provide a basis for the experimental breadth of the spin-allowed bands as $^3A_2 \rightarrow {}^3T_2$ is at 16 045 – 16 175 cm^{-1}, $^3A_2 \rightarrow {}^1T_2(D)$ is at 20 570 – 20 600 cm^{-1}, which is not too far from the proposed spin-forbidden shoulders, and $^3A_2 \rightarrow {}^3T_1(P)$ is at 33 915 – 34 065 cm^{-1}. These results, calculated using Ligfield[24] are given in Table S5a.

b) Discussion of electronic spectra of $M(NR_2)_4$ complexes, R = Me, Et; M = Cr, Mo.

None of the green amido complexes, $Cr(NR_2)_4$, was structurally characterized or produced X-band EPR spectra.[11] That with R = Et gave a single, strong (ε = 1200) visible band at 13 700 cm^{-1} (730 nm) and its possible assignment to one of the three d-d transitions described above was thoughtfully considered,[11] with no assignment being ideal. This band is much red-

shifted from the corresponding major band seen in CrR_4 (~500 nm), so that the same assignment ($^3A_2 \rightarrow {}^3T_1(F)$) also with B = 450 cm^{-1} gives ε_σ = 7067 cm^{-1} (Dq = 9423 cm^{-1}), which is unreasonably low.[11] If this band is assigned to $^3A_2 \rightarrow {}^3T_2$, then Dq = 1370 cm^{-1} (or ε_σ = 10 275 cm^{-1}), which is reasonable in comparison to the larger value for the stronger-field alkyl donors. The mystery is that the allowed $^3A_2 \rightarrow {}^3T_1(F)$ transition would be well within the visible region for any realistic value of B, e.g., in the range 17 960 – 18 810 cm^{-1} (~560 – 530 nm) for B = 400 – 500 cm^{-1}, and thus should be readily observable – more so than the forbidden $^3A_2 \rightarrow {}^3T_2$ transition. The $^3A_2 \rightarrow {}^3T_1(P)$ transition would be above 29 000 cm^{-1} and obscured by charge-transfer bands.

Intrigued by this difficulty, we also considered the structurally characterized complex $Mo(NMe_2)_4$, which has D_{2d} symmetry, and a singlet ground state ($^1A_1$, $d_{x^2-y^2}{}^2\left(b_1^2\right)$) with a more informative electronic absorption spectrum.[25] An AOM fit of this system was successful, albeit not a unique solution, using their assignment of bands at 10 500 cm^{-1} to $^1A_1 \rightarrow {}^1B_1$ ($d_{x^2-y^2}\left(b_1\right) \rightarrow d_{z^2}\left(a_1\right)$; forbidden in D_{2d}), 14 300 cm^{-1} to $^1A_1 \rightarrow {}^1E$ ($\rightarrow d_{xz,yz}\left(e\right)$; xy allowed), and ~ 20 000 cm^{-1} to $^1A_1 \rightarrow {}^1A_2$ ($\rightarrow d_{xy}\left(b_2\right)$; forbidden). The fit results are given in Table S3 and the energy levels with free-ion parentage are given in Table S4. The AOM included π-donation in the proper orientation (i.e., normal to the NEt_2 plane; $\varepsilon_{\pi-c}$ = 5162.2 cm^{-1}) with ε_σ = 11 876.4 cm^{-1} – a reasonable value for the strong σ-donor amido ligand. The Racah parameter B was 484.4 cm^{-1}; ~70% of the free-ion value, with C fixed at C/B = 4.47, also based on the free-ion value.[26-27] We thus favor the assignment of the single band for $Cr(NEt_2)_4$ to $^3A_2 \rightarrow {}^3T_2$, but have no explanation from LFT for the absence of the other expected bands.

c) Discussion of electronic spectrum of $Cr(O^tBu)_4$.

In contrast to the amido complexes, $Cr(O^tBu)_4$ displayed a relatively informative electronic absorption spectrum.[7] Bands centered at 9100 cm^{-1} (ε = 10), 15 200 cm^{-1} (ε = 560), and 25 000 cm^{-1} (sh, $\varepsilon \approx 500$) were observed and assigned respectively to $^3A_2 \rightarrow {}^3T_2$, $^3A_2 \rightarrow {}^3T_1(F)$, and $^3A_2 \rightarrow {}^3T_1(P)$, analogously to the tetraalkyls described above. In T_d symmetry, these three bands can be fitted (each to within 200 cm^{-1}) using: B = 816.8 cm^{-1} (~80% of the free-ion value[20]), Dq = 927.4 cm^{-1}.[28] Use of the AOM with T_d symmetry and only σ-bonding analogously gives B = 816.4 cm^{-1}, ε_σ = 6954.5 cm^{-1}.

One can next use experimentally determined structures, rather than ideal T_d symmetry. There is no reported structure of $Cr(O^tBu)_4$, but we can use that for $Cr(OCH^tBu_2)_4$,[29]with idealized D_{2d} symmetry (average $\angle$O-Cr-O = 111.4°; relevant metrics are given in Table S1. The slight tetragonal compression of this complex is reflected in the following angles: 112.45°, 110.36°, 108.75° × 2, 108.27° × 2, thus nearly defining an S_4 axis. This AOM fits the observed bands moderately well using B = 817.2 cm^{-1}, ε_σ = 6961.3 cm^{-1}. In addition to this use of a more realistic structure, one can include π-donation by the alkoxide ligands, which was not appropriate for the alkyls. This bonding type, however, has little effect. If only $\varepsilon_{\pi-s}$ is included, then its value is driven to zero; if only $\varepsilon_{\pi-c}$ is included, then the fit yields only a very modest value (140 cm^{-1}); the resulting energy levels are given in Table S3. If cylindrical π-bonding is included, then the fitting simply drives the π-bonding to zero, giving essentially the same result as with only σ-bonding. Thus, use of an experimentally based geometry and inclusion of π-bonding have little effect so that the alkoxides behave functionally the same as alkyls: strong σ-donors with slight distortion from ideal tetrahedral symmetry due to ligand steric effects.

d) Discussion of electronic spectrum of $Cr(DTBMS)_4$.

An alternate crystal field model for $Cr(DTBMS)_4$ from that described in the main text is to assume that the $^3A_2 \rightarrow {}^3T_1(P)$ transition is above ~22 000 cm^{-1} (below 450 nm), i.e., obscured by the edge of the intense CT band. If we assign this transition to a hypothetical band at 22 700 cm^{-1} (440 nm), then the three spin-allowed transitions are each fitted to within ~400 cm^{-1} using B = 792 cm^{-1} and Dq = 773 cm^{-1}. This tetrahedral crystal field splitting is close to that in the preferred model, i.e., that described in the main text, while the B parameter is more consistent with that for $Cr(O^tBu)_4$ and is not so reduced from the free-ion value. For illustration we present in Figure S1 an energy level diagram analogous to that shown in Figure 5, but here with B = 800 cm^{-1} and C = 3300 cm^{-1} (so as to use round numbers; C/B = 4.125, versus 4.11 in the free-ion[20]).

To apply the AOM, we note that the O-Cr-O angles in $Cr(DTBMS)_4$ are: 108.02° (×2), 108.21° (×2), 111.83°, and 112.61°. The four essentially identical angles (crystallographic two-fold axis) define the S_4 axis in D_{2d} idealized symmetry, and we then use the average of the two larger angles: 112.22°, so that two siloxide O donors are at θ = 56.11°, and two are at θ = 123.89°. The x axis is chosen to lie between the Cr-O bonds (along C_2'). $Cr(DTBMS)_4$ thus exhibits a slightly "squashed" tetrahedral geometry, very slightly more so than $Cr(OCH^tBu_2)_4$ (see Tables S1 and S2),[29] but much less than $Cr(N{=}C^tBu_2)_4$, for which the angles are roughly 98° (×4) and 136° (×2) (so θ = 68°).[30]

We then fit the observed electronic transitions as before, except now only the central of the three orbital terms of the $^3T_{1,2}$ parent term in T_d is used, i.e., we make no determination as to $^3B_1 \rightarrow {}^3E(^3T_2(F))$ versus $^3B_1 \rightarrow {}^3B_2(^3T_2(F))$. However, in D_{2d} the former is x,y-dipole-allowed but the latter is forbidden, so the latter is more likely that which is observed. It is possible using only σ-bonding to match the spin-allowed transitions quite closely, and subsequent adjustment of the

Racah *C* parameter allows fitting the spin-forbidden band at 540 nm. This model can be further refined by inclusion of a small degree of π-donation by the siloxido ligands, as given by $\varepsilon_{\pi-c}$ = 230 cm^{-1}, together with ε_{σ} = 6600 cm^{-1}. It is thus possible to fit all of the originally assigned spin-allowed and -forbidden transitions exactly, as summarized in Table S3. The ligand-field energy levels, with free-ion parentage, for both the favored (in main text; Tanabe-Sugano diagram in Figure 5) and disfavored (that described here; Tanabe-Sugano diagram in Figure S1) models of $Cr(DTBMS)_4$ are given in Table S4. We do not claim that either is a unique solution, but the AOM can minimally provide a reasonable description of the electronic structure of this complex. The SOC interaction can then be included so as to reproduce the experimental zfs. Use of ζ = 198 cm^{-1} (62% of the free-ion value[23]) exactly reproduces the zfs of the major component (B), D = +0.565 cm^{-1}. The results of this calculation for the preferred (main text) model are given in Table S5b. The ζ parameter can be increased or decreased to match the D value of components A or C, respectively. Another, more physically attractive way to model the several species is to alter slightly the AOM. The bonding parameters have been maintained as the same among the four ligands; this may not necessarily be the case, but since the four Cr-O bond lengths are essentially identical, we shall explore only slight angular changes. For example, if θ is changed from the crystallographically determined average value of 56.11° by only *one* degree to 57.11° (i.e., a slight increase in tetragonal distortion – "squashing"), then the D value increases to +0.81 cm^{-1}, a value already greater than that determined for component A. We also note than an idealized D_{2d} symmetry has been used thus far. If the real, rather than average θ values are used, then D = +0.566 cm^{-1}, essentially the same, but now with $|E|$ = 0.01 cm^{-1} ($|E/D|$ = 0.02). But if the ϕ angle of a pair of ligands is changed by only one degree from ideal S_4 (i.e., to 45°, 134 °, 225°, 314°) then the D value is unchanged, but $|E|$ increases to 0.062 cm^{-1}, ($|E/D|$ = 0.11).

The point is that the zfs is very sensitive to small changes in geometry and a four-coordinate geometry is inherently susceptible to small distortions of the type described here – changes on the order of one degree can lead to the variation in zfs observed for the several components seen for $Cr(DTBMS)_4$. These geometrical effects are explored more extensively using QCT and shown graphically in Figures S11 and S12.

Lastly, one can also use the second set of assignments, i.e., that with the larger B value (Figure S1), also with the AOM, but then the $^3B_1 \rightarrow {}^3E(^3T_2(F))$ transition is always higher in energy than $^3B_1 \rightarrow {}^3B_2(^3T_2(F))$, so that a negative D value obtains (see Eqn 4). The magnitude of D is also too low unless an unreasonably large (i.e., essentially the free-ion value) for ζ is employed. Therefore, the constraints from zfs parameters, extracted by HFEPR, allows a seemingly reasonable set of assignments for electronic transitions to be discarded.

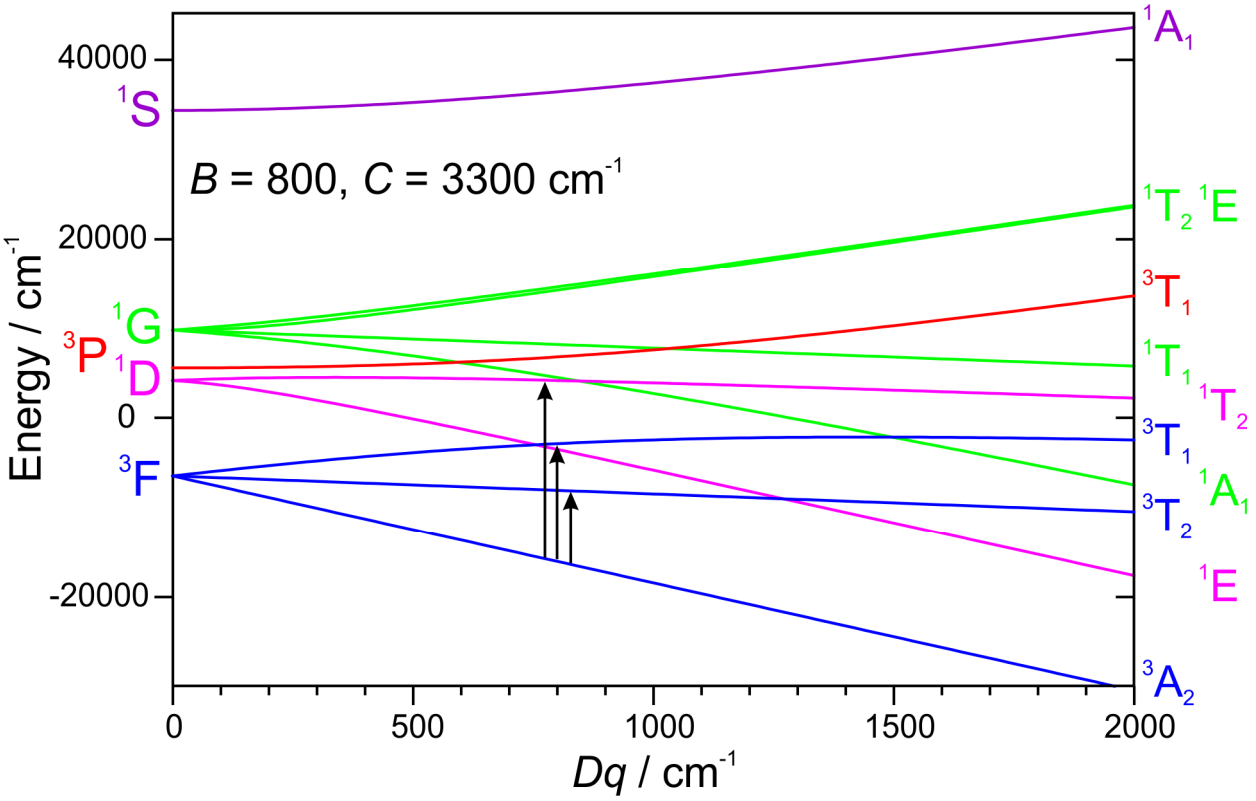

Figure S1. Energy diagram for $Cr(DTBMS)_4$ generated using Racah parameters B = 800 cm^{-1}, C = 3300 cm^{-1} and the tetrahedral crystal field splitting range as indicated on the abscissa. The three vertical arrows represent possible assignments using $Dq \approx 800$ cm^{-1} of the three transitions observed at (left to right) 18 520 cm^{-1} (540 nm), 12 500 cm^{-1} (800 nm), and 8070 cm^{-1} (1240 nm).[14] The electronic transitions are matched as shown here, but the AOM when applied to this parameter set does not reproduce the observed zfs of $Cr(DTBMS)_4$, giving the incorrect sign of D. The analogous diagram that matches both optical and HFEPR spectroscopic data is shown in Figure 5 (main text), and is thus the preferred model. The ligand-field energy levels of the disfavored model shown here and the favored model (Figure 5) are listed in Table S4 with their free-ion parentage.

e) Discussion of putative electronic spectrum of molecular CrF_4.

The final compound is the fluoride, molecular CrF_4. For the synthesis of this species, one can go far back in the literature,[31] as well as more recently.[32] This paper by von Wartenberg even reported a gas phase absorption spectrum,[31] but this spectrum was likely due to a dimer,[33] as later suggested by the electronic absorption spectrum of authentic CrF_4 isolated in a neon matrix,[34]

which shows no absorption beyond 450 nm.[35] For illustrative purposes, if we simply define the transition $^3A_2 \rightarrow {}^3T_1(P)$ as being at 400 nm, then this band can be fitted using B = 964 cm^{-1}, ε_σ = 8165 cm^{-1}, and ε_π = 1633 cm^{-1}, where $\varepsilon_{\pi-c} \equiv \varepsilon_{\pi-s} = \varepsilon_\pi \equiv \varepsilon_\sigma/5$; admittedly all arbitrary, but reasonable, which parameter set gives $^3A_2 \rightarrow {}^3T_1(F)$ at 745 nm and $^3A_2 \rightarrow {}^3T_2$ at 1290 nm, both of which bands might not be observed in the visible spectrum in a matrix. The electronic spectrum of CrF_4 is examined by QCT methods (see Table S10 and Figure S15).

f) Further discussion of perturbation theory equations for spin Hamiltonian parameters.

Mowat et al.[3] gave a further expression for D by including values for the energy denominators in Eqn 4 (see main text) and combining like terms. Their result is given below:

$$D \approx \zeta^2\delta\left\{\frac{1}{\Delta^2}-\frac{1}{\left[\Delta+8B+2C\right]^2}\right\}-2\zeta\left(\zeta_{\parallel}-\zeta_{\perp}\right)\left\{\frac{1}{\Delta}-\frac{1}{\left[\Delta+8B+2C\right]}\right\} \qquad \text{(S1)}$$

where Δ is the tetrahedral splitting (10Dq), δ is the tetragonal splitting, and $\zeta_{\parallel}$ and $\zeta_{\perp}$ are the SOC constants in the parallel (collinear with z) and perpendicular directions, respectively. For a CrR_4 complex, Mowat et al. used for illustration Δ = 14 500 cm^{-1}, δ = 2500 cm^{-1}, $B = C/4$ = 450 cm^{-1}, and ζ = 104 cm^{-1}, which is only one third of the free-ion value. These values give $D \approx 0.07$ cm^{-1}, using only the first part of Eqn S1 (i.e., assuming isotropic SOC), which is in the range of the small zfs seen for tetraalkylchromium(IV) complexes. The problem is that the second part of Eqn S1 could range from zero to a magnitude as large as the first part depending on how much SOC anisotropy one wishes to introduce. We have explored this using a spreadsheet and find that anywhere in the range $-0.06 < D < +0.07$ cm^{-1} is readily achievable. Moreover, the denominator for the $^1T_2$ excited state energy is based only on diagonal matrix elements, as given by McClure[36]), which give the $^3A_2$ ground state at ($-8B - 12Dq$) and a $^1T_2$ excited state at ($2C - 2Dq$), so the energy difference is indeed ($2C + 8B + 10Dq$). The problem here is that this $^1T_2$ state

actually corresponds in the strong-field limit to $e^0t_2^2$, which is not an accessible excited state; the correct $^1T_2$ state, which is $e^1t_2^1$ in strong field notation is at $(B + 2C)$, based only on diagonal elements. Using an exact calculation with the Dq, B, and C parameters of Mowat et al.[3] puts the correct $^1T_2$ excited state (of roughly two thirds ^1D and one third ^1G free-ion parentage) at 21 539 cm^{-1}, rather than 21 700 cm^{-1}, so that everything works out in the end. Nevertheless, if we use only the first part of Eqn S1 with $\Delta \approx 8000$ cm^{-1}, $\delta \approx 1000$ cm^{-1} (based on the splitting within the $^{1,3}T_2$ states using the AOM) and the energy of the $^1T_2$ excited state calculated exactly (in T_d symmetry) at 16 020 cm^{-1} (also see Figure 5), then with $190 \leq \zeta \leq 255$ cm^{-1} (60 – 80% of the free-ion value[23]), the experimental range of D values is reproduced. Alternatively, and perhaps more realistically, the tetragonal distortion can be varied, with ζ fixed at 60% of the free-ion value. The range of $1000 \leq \delta \leq 1700$ cm^{-1} then covers the experimental range of D values. This exercise provides a semi-quantitative basis for the several species seen by HFEPR, namely a small change in tetragonal distortion.

Table S1. CrL_4 ($Cr(ER_n)_4$, n = 0 – 3, E = F, O, N, C) metrical parameters from X-ray diffraction and DFT geometry optimization.[a]

Complex	d Cr-E (Å)	∠ E-Cr-E (deg.)
CrF_4 – expt.[37]	1.706(2)	essentially T_d symmetry (109.5)
CrF_4 – optimized triplet	1.714	109.4 × 2, 109.5 × 3, 109.6
CrF_4 – optimized singlet	1.713	109.3 × 3, 109.4, 109.7, 109.8
Alkyls		
$Cr(cHx)_4$ – expt.[38b]	2.010 × 4	106.2 × 2, 107.8 × 2, 114.5, 114.6
$Cr(^tBu)_4$ – optimized triplet	2.014 × 4	109.5 × 6
$Cr(^tBu)_4$ – optimized singlet	2.082, 2.084, 2.085, 2.086	109.2, 109.4, 109.5, 109.6 × 3
$Cr(CH_2SiMe_3)_4$ – optimized triplet	1.999, 2.001, 2.002 × 2	107.6, 108.7, 108.9, 109.2, 110.9, 111.4
$Cr(CH_2SiMe_3)_4$ – optimized singlet	1.988 × 2, 1.989 × 2	107.9, 108.2, 109.3, 110.0. 110.2, 111.2
Amidos		
$Cr(NMe(CH^tBu_2))_4$ – optimized triplet[38]	1.946, 1.952, 1.960. 1.972	105.3, 105.8, 107.7, 108.1, 114.0. 116.3
$Cr(NMe(CH^tBu_2))_4$ – optimized singlet	1.919 × 2, 1.932, 1.939	101.6, 104.4, 110.9, 111.0. 112.4, 116.8
$Cr(NMe_2)_4$ – optimized triplet, no symmetry restrictions	1.856 × 2, 1.857 × 2	102.9 × 2, 112.8, 112.9 × 3
$Cr(NMe_2)_4$ – optimized singlet, preserved C_2 symmetry	1.835 × 4	108.2, 108.3, 108.4 × 2, 111.8 × 2
Alkoxides		
$Cr(OCH^tBu_2)_4$ – expt.[29]	1.771 × 2, 1.775 × 2	108.3 × 2, 108.8 × 2, 110.4, 112.4
$Cr(OCH^tBu_2)_4$ – optimized triplet	1.782 × 4	107.9 × 4, 112.6 × 2
$Cr(OCH^tBu_2)_4$ – optimized singlet	1.778 × 4	108.2 × 4, 112.1, 112.2
$Cr(O^tBu)(OCMe^tBu_2)_3$ – expt.[39]	1.740. 1.781, 1.782, 1.796	105.6, 105.6, 107.5, 112.2, 112.3, 113.2
$Cr(O^tBu)_4$ – optimized triplet	1.772 × 4	106.5 × 4, 115.6 × 2
$Cr(O^tBu)_4$ – optimized singlet	1.766 × 3, 1.767	108.0 × 4, 112.5 × 2
$Cr(OMe)_4$ – optimized triplet	1.758, 1.764, 1.767, 1.774	103.8, 107.3, 110.6, 110.8, 111.8, 112.2
$Cr(OMe)_4$ – optimized singlet	1.760 × 4	109.1, 109.2, 109.3, 109.5, 109.8 × 2
Siloxides		
$Cr(DTBMS)_4$ – expt.[14]	1.764 × 2, 1.765 × 2	108.0 × 2, 108.2 × 2, 111.8, 112.6
$Cr(DTBMS)_4$ – optimized triplet, triplet ground state	1.772 × 4	111.0. 110.9, 108.7, 108.8 × 3
$Cr(DTBMS)_4$ – optimized singlet	1.770 × 4	108.6, 108.8, 109.1, 109.2, 110.5, 110.6
$Cr(OSiMe_3)_4$ – optimized triplet, preserved C_2 symmetry	1.760 × 4	108.5 × 4, 111.4 × 2
$Cr(OSiMe_3)_4$ – optimized singlet	1.757 × 4	109.1 × 4, 110.1 × 2

[a] See Table S2 for a continuous shape measures analysis that quantifies the deviation from ideal tetrahedral geometry for many of the complexes in this table.[14, 39]
[b] cHx = cyclohexyl.

Table S2. Continuous shape measures analysis of selected $[ML_4]^{0,-}$ complexes (M = Cr^{IV}, V^{III}).

S H A P E v2.1 Continuous Shape Measures calculation

(c) 2013 Electronic Structure Group, Universitat de Barcelona, Contact: llunell@ub.edu

SP-4 1 D_{4h} Square (Here, CShM = 33.3 corresponds to ideal T_d; zero to ideal square); calculated *x*, *y*, *z* coordinates are given.

T-4 2 T_d Tetrahedron (Here, CShM = 0 corresponds to ideal T_d); calculated *x*, *y*, *z* coordinates are given.

	1	[SESROZ_cleaned]			SP-4	31.1		T-4	0.058	
Cr		5.638	-6.078	-0.276	5.634	-6.078	-0.276	5.634	-6.078	-0.276
O1		6.616	-7.545	-0.276	5.634	-7.542	-0.274	6.652	-7.518	-0.274
O2		4.649	-6.081	-1.737	5.634	-6.079	-1.740	4.615	-6.079	-1.716
O1		6.616	-4.610	-0.276	5.633	-4.613	-0.277	6.652	-4.637	-0.277
O2		4.649	-6.074	1.186	5.634	-6.076	1.189	4.615	-6.076	1.165
	2	[ALUHOF_ortho]			SP-4	32.9		T-4	0.084	
Cr		-17.192	-10.673	-17.780	-17.219	-10.731	-17.778	-17.219	-10.731	-17.778
O		-16.200	-12.153	-17.780	-17.209	-12.183	-17.773	-16.152	-12.146	-17.781
O		-16.222	-9.228	-17.780	-17.230	-9.278	-17.783	-16.241	-9.253	-17.790
O		-18.259	-10.810	-19.217	-17.237	-10.736	-19.230	-18.253	-10.767	-19.218
O		-18.224	-10.790	-16.332	-17.201	-10.726	-16.325	-18.232	-10.757	-16.323
	3	[LIBCRB_ortho]			SP-4	31.8		T-4	0.034	
C		6.945	-2.708	-9.235	6.945	-2.715	-9.227	6.945	-2.715	-9.227
O		7.977	-4.148	-9.235	7.974	-3.457	-9.959	7.975	-4.157	-9.213
O		7.979	-1.265	-9.235	7.987	-1.964	-8.524	7.962	-1.263	-9.269
O		5.940	-2.671	-7.777	5.916	-1.973	-8.495	5.942	-2.691	-7.766
O		5.886	-2.783	-10.656	5.903	-3.466	-9.931	5.902	-2.748	-10.660
	4	[FEFTUF]			SP-4	29.2		T-4	0.203	
Cr		-2.062	0.521	3.829	-2.062	0.520	3.829	-2.062	0.520	3.829
C		-0.441	1.607	4.312	-0.437	0.520	4.296	-0.486	1.679	4.282
C		-1.611	-0.566	2.200	-1.595	0.520	2.204	-1.609	-0.639	2.254
C		-3.682	1.607	3.347	-3.687	0.520	3.362	-3.638	1.679	3.377
C		-2.513	-0.566	5.459	-2.529	0.520	5.454	-2.515	-0.639	5.405
	5	[Cr(OSiMe^{t}Bu$_2$)]			SP-4	32.1		T-4	0.016	
Cr		-0.001	0.001	0.001	0.000	0.001	0.001	0.000	0.001	0.001
O		-1.371	0.558	0.975	-1.394	0.433	-0.021	-1.358	0.557	0.994
O		-0.455	-1.507	-0.811	-0.431	-1.381	0.185	-0.451	-1.497	-0.830
O		1.417	-0.303	1.019	1.394	-0.430	0.023	1.405	-0.298	1.037
O		0.408	1.258	-1.180	0.430	1.384	-0.183	0.403	1.243	-1.196
	6	[Cr(O^{t}Bu)$_4$]			SP-4	28.4		T-4	0.287	
Cr		0.000	0.000	0.000	0.000	0.000	0.000	0.000	0.000	0.000
O		1.097	0.128	-1.386	0.596	-0.653	-1.211	1.116	0.215	-1.356
O		0.622	-1.313	1.014	1.123	-0.532	0.839	0.540	-1.358	0.998
O		-0.094	1.434	1.036	-0.595	0.653	1.211	-0.032	1.474	0.978
O		-1.623	-0.249	-0.665	-1.123	0.532	-0.839	-1.624	-0.332	-0.620

7	[Cr(OCH^{t}Bu$_2$)$_4$]			SP-4	30.7		T-4	0.077	
Cr	0.000	0.000	0.000	0.000	0.000	0.000	0.000	0.000	0.000
O	0.683	1.501	-0.676	0.982	0.597	-0.938	0.651	1.527	-0.647
O	-0.718	-0.927	-1.342	-1.017	-0.023	-1.079	-0.687	-0.964	-1.331
O	-1.280	0.308	1.201	-0.982	-0.597	0.938	-1.274	0.356	1.193
O	1.316	-0.881	0.816	1.017	0.023	1.079	1.309	-0.919	0.785
8	[Cr(OMe)$_4$]			SP-4	31.8		T-4	0.104	
Cr	0.046	-0.105	-0.091	0.005	-0.110	-0.074	0.005	-0.110	-0.074
O	0.018	-1.232	-1.441	-0.283	-0.288	-1.492	0.040	-1.247	-1.423
O	0.552	-0.890	1.409	0.293	0.068	1.344	0.612	-0.904	1.380
O	1.040	1.301	-0.476	1.347	0.355	-0.404	1.021	1.282	-0.451
O	-1.631	0.377	0.228	-1.336	-0.575	0.256	-1.653	0.428	0.198
9	[Cr^{t}Bu$_4$]			SP-4	33.3		T-4	0.000	
Cr	0.000	0.000	0.000	0.000	0.000	0.000	0.000	0.000	0.000
C	-0.482	-1.748	-1.088	-1.235	-0.805	-0.899	-0.481	-1.748	-1.088
C	-1.322	0.197	1.638	-0.570	-0.745	1.449	-1.322	0.197	1.638
C	1.986	-0.137	0.711	1.235	0.804	0.899	1.986	-0.137	0.710
C	-0.183	1.687	-1.260	0.570	0.745	-1.449	-0.183	1.687	-1.260
10	[Cr(NMe$_2$)$_4$]			SP-4	30.8		T-4	0.328	
Cr	0.000	-0.001	-0.001	0.000	-0.001	0.000	0.000	-0.001	0.000
N	0.147	1.095	-1.491	0.876	1.014	-0.767	0.064	1.149	-1.453
N	-1.670	-0.799	0.147	-0.876	-1.016	0.766	-1.651	-0.841	0.051
N	1.368	-1.232	-0.254	0.554	-1.143	-0.880	1.336	-1.276	-0.162
N	0.156	0.932	1.597	-0.554	1.141	0.879	0.252	0.963	1.563
11	[Cr(NMe-CH^{t}Bu$_2$)]			SP-4	28.8		T-4	0.259	
Cr	-0.005	-0.014	0.013	-0.005	0.002	0.022	-0.005	0.002	0.022
N	0.443	1.888	-0.254	0.635	1.149	-0.980	0.387	1.907	-0.179
N	-0.875	-0.394	1.728	-0.646	-1.145	1.024	-0.850	-0.310	1.757
N	1.704	-0.956	-0.021	1.481	-0.234	0.702	1.657	-1.021	-0.087
N	-1.293	-0.515	-1.358	-1.492	0.237	-0.659	-1.216	-0.568	-1.404
12	[CrF$_4$]			SP-4	33.3		T-4	0.000	
Cr	0.001	0.000	0.001	0.000	0.000	0.000	0.000	0.000	0.000
F	0.200	1.550	0.706	0.927	0.900	0.538	0.200	1.548	0.707
F	-1.654	-0.252	-0.369	-0.927	-0.901	-0.538	-1.655	-0.251	-0.369
F	0.926	-0.095	-1.439	0.198	0.554	-1.270	0.926	-0.095	-1.439
F	0.528	-1.204	1.100	-0.199	-0.554	1.270	0.529	-1.203	1.100
13	[OCEWIC]			SP-4	27.8		T-4	0.803	
V	6.546	2.288	8.460	6.567	2.291	8.449	6.567	2.291	8.449
C	5.101	0.704	8.435	5.225	1.418	7.570	5.246	0.607	8.492
C	7.938	2.143	6.816	7.805	1.289	7.555	7.789	2.195	6.694
C	7.977	2.309	10.067	7.909	3.164	9.328	7.814	2.265	10.189
C	5.273	4.012	8.468	5.329	3.293	9.343	5.419	4.098	8.421

Table S3. LFT fit results for electronic absorption bands of CrL_4 complexes. All energies in cm^{-1}.

Complex	Dataset / Model	Band assignment in T_d symmetry from $^3A_2(F)$ ground state			
$Cr(Nor)_4$		$\rightarrow {}^3T_2(F)$	$\rightarrow {}^3T_1(F)$ [a]	$\rightarrow {}^3T_1(P)$ [a]	$\rightarrow$ singlets [b]
	Expt.[c]	16 130	20 580	(CT at 29 850. 34 010)	18 730. 18 080
	Crystal-field, AOM [d]	16 130	20 580	33 960	6590. 12 250. 22 660. 24 420
$Cr(NEt_2)_4$					
	Expt.[e]	13 700	---	(CT at 25 000 – 50 000)	---
	Crystal-field, AOM [f]	13 700	18 810	29 790	8000. 14 480. 21 600. 23 810
$Cr(O^tBu)_4$					
	Expt.[g]	9100 (8700. 9500)	15 200	25 000 (CT at 37 000. 45 000)	---
	Crystal-field [h]	9270 (9430)	15 040 (15 200)	25 030 (25 000)	12 850. 21 300. 21 790 (12 490. 20 820. 21610)
	AOM [i]	9040. 9730 (9090. 10 160)	14 990. 15 100 (15 230. 15 240)	24 960. 25 080 (24 940. 25 220)	12 840. 12 860. 21 300. 21 580. 22 180 (12 590 × 2, 21 000. 21 410. 22 360)
$Cr(OSiMe^tBu_2)_4$ = $Cr(DTBMS)_4$		$\rightarrow {}^3T_2(F)$	$\rightarrow {}^3T_1(F)$ [a]	$\rightarrow {}^3T_1(P)$ [a]	$\rightarrow$ singlets [b]
	Expt.[j]	8070	12 500	--- (CT at 36 000)	9600. 18 520
	Crystal-field [k]	8070 (7730)	12 500 (12 770)	19 670 (22 300)	8127, 14 016, 16 020. 18 520 (12 400. 23 740)
	AOM [l]	8070. 8966 (8069, 9599)	12 500. 12 950 (12 499, 12 785)	19 442, 19 912 (19 084, 19 851)	8039, 8049, 13 795, 15 986, 16 820. 18 238, 19 092 (7645, 7703, 13 251, 15 668, 17 142, 17 968, 18 520. 24 867)

[a] The free-ion parentage of these terms is very mixed and the lower energy term can in some cases have a higher ^3P parentage, while the higher energy term correspondingly has a higher ^3F parentage, but we label

all of these respectively as from ^{3}F and ^{3}P to correspond with the traditional Tanabe-Sugano diagram (see Figures 5 and S1).

[b] The specific singlet excited states are defined in each case, where applicable. Only those below ~25 000 in energy ($\lambda > 400$ nm) are given; more complete listings are given in Tables S4 – S5.

[c] Data taken from Abrahamson et al.[18] The strong bands in the UV were assigned to charge transfer (CT), but could include d-d transitions. The spin-forbidden transitions were assigned to $^3A_2(F) \rightarrow {}^1E(D)$, but this is calculated here to be much too low in energy (6950 cm^{-1}) to be observable. We suggest that these shoulder features may be due in part to $^3A_2(F) \rightarrow {}^1A_1(G)$ (calculated at 12 250 cm^{-1}) and/or $^3A_2(F) \rightarrow {}^1T_2(D)$ (calculated at 22 660 cm^{-1}).

[d] The parameters (in cm^{-1}) used in the crystal-field model are: Racah B = 410. C = 1685 (set at 4.11B), Dq = 1613. Those in the AOM are: Racah as with crystal-field, ε_σ = 12 097.5, with AOM geometry (ideal tetrahedral; no structure is available): θ = 54.736° (× 2), 125.264° (× 2), ϕ = 45° and 225°, 135° and 315°.

[e] Data taken from Basi et al.[11] Only one band was observed (at 730 nm).

[f] The parameters (in cm^{-1}) used in the crystal-field model are: Racah B = 500. C = 2055 (set at 4.11B), Dq = 1370. Those used in the AOM are: Racah as with crystal-field, ε_σ = 10 275.0. with AOM geometry (ideal tetrahedral since no structure is available): θ = 54.736° (× 2), 125.264° (× 2), ϕ = 45° and 225°, 135° and 315°. Alternate assignments of the single observed band gave less reasonable parameters. Moreover, the AOM parameters are consistent with those derived for the structurally characterized,[25] ground state singlet molecule $Mo(NMe_2)_4$ (see Table S4c).

[g] Data taken from Alyea et al.[7] For the lowest energy band, the center of gravity is used for crystal-field and initial AOM fitting, but two bands (given in parentheses) were observed, due to tetragonal distortion from tetrahedral symmetry.

[h] The parameters (in cm^{-1}) used in the crystal-field model are in two sets; one is a consensus fit for all three bands, while the other (calculated band energies and parameters in parentheses), matches the two higher energy bands exactly but the lowest less well: Racah B = 816.4 (794), C = 3355.0 (3260; both set at 4.11B), Dq = 927.7 (943).

[i] The parameters (in cm^{-1}) used in the AOM are in two sets; one with only σ-bonding, while the other (calculated band energies and parameters in parentheses) includes π-bonding: Racah B = 817.2 (800.6), C = 3360 (3290; both set at 4.11B), ε_σ = 6961.3 (7185.7; $\varepsilon_{\pi\text{-c}}$ = 139.3), with AOM geometry based on the reported crystal structure for $Cr(OCH^tBu_2)_4$,[29] with idealized D_{2d} symmetry: θ = 55.7° (× 2), 124.3° (× 2), ϕ = 45° and 225°, 135° and 315°.

[j] Data taken from Marshak and Nocera.[14]

[k] The parameters (in cm^{-1}) used in the crystal-field model are in two sets; one with no assumptions as to the $^3A_2 \rightarrow {}^3T_1(P)$ transition (i.e., that in the main text, see Figure 5), and one (calculated band energies and parameters in parentheses) where this transition is presumed to be at 22 700 cm^{-1} (i.e., that described in SI, see Figure S1, which is disfavored due to inconsistency with the observed positive D value): Racah B = 530.7 (792.0), C = 2040.8 (C/B = 3.84) (3255; set at 4.11B), Dq = 807.0 (773.0).

[l] The parameters (in cm^{-1}) used in the AOM are in two sets; one with only σ-bonding, while the other (calculated band energies and parameters in parentheses) includes π-bonding: Racah B = 486.6 (427.5), C = 2157.4 = 4.43B (2206.0 = 5.16B), ε_σ = 6294.0 (6600.0; $\varepsilon_{\pi\text{-c}}$ = 230.0), with AOM geometry based on the reported crystal structure,[14] with idealized D_{2d} symmetry: θ = 56.11° (× 2), 123.89° (× 2), ϕ = 45° and 225°, 135° and 315°.

Table S4. LFT term relative energy level output for selected ML_4 (M = Cr^{IV}, Mo^{IV}) complexes. All energies in cm^{-1}.

Complex, model used	Term number	Relative energy [a]	Description in T_d (with free-ion parentage)[b]	Description in D_{2d}
a) $Cr(Nor)_4$				
calculated using crystal-field model with: B = 410. C = 1685, Dq = 1613.	1 – 3	0.0	$^3A_2$(F)	---
	4 – 5	6588.4	^1E (D 60%, G 40%)	---
	6	12 248.8	$^1A_1$(G 75%, S 25%)	---
	7 – 15	16 130.0 (obs)	$^3T_2$(F)	---
	16 – 24	20 581.2 (obs)	$^3T_1$(F 35%, P 65%)	---
	25 – 27	22 658.9	$^1T_2$(D 65%, G 35%)	---
	28 – 30	24 420.0	$^1T_1$(G)	---
	31 – 39	33 958.8	$^3T_1$(F 65%, P 35%)	---
	40 – 41	39 381.6	^1E (G 60%, D 40%)	---
	42 – 44	39 441.1	$^1T_2$(G 65%, D 35%)	---
	45	49 116.2	$^1A_1$(S 75%, G 25%)	---
b) $Cr(NEt_2)_4$				
calculated using AOM with ideal Td geometry with: B = 500. C = 2055, ε_σ = 10 275.	1 – 3	0.0	$^3A_2$(F)	---
	4 – 5	8002.9	^1E (D 60%, G 40%)	---
	6 – 14	13 700.0 (obs)	$^3T_2$(F)	---
	15	14 480.6	$^1A_1$(G 80%, S 20%)	---
	16 – 24	18 808.2	$^3T_1$(P 50%, F 50%)	---
	25 – 27	21 601.8	$^1T_2$(D 70%, G 30%)	---
	28 – 30	23 810.0	$^1T_1$(G)	---
	31 – 39	29 791.8	$^3T_1$(F 50%, P 50%)	---
	40 – 41	36 117.1	^1E (G 60%, D 40%)	---
	42 – 44	36 218.2	$^1T_2$(G 70%, D 30%)	---
	45	48 414.4	$^1A_1$(S 80%, G 20%)	---
c) $Mo(NMe_2)_4$				
Complex, model used	Term number	Relative energy [a]	Description in T_d (with free-ion parentage)[b]	Description in D_{2d}
calculated using AOM with ideal D_{2d} geometry with: B = 484.4, C = 2093.9, ε_σ = 11 876.4, $\varepsilon_{\pi\text{-}c}$ = 5162.2	1	0.0	^1E (D 50%, G 40%, S 10%)	$^1A_1$
	2 – 4	2692.0	$^3A_2$(F)	$^3B_1$
	5 – 10	7039.7	$^3T_2$(F)	^3E
	11	10 500.4 (obs)	^1E (D 65%, G 35%)	$^1B_1$
	12 – 13	14 300.0 (obs)	$^1T_2$(D 50%, G 50%)	^1E
	14 – 16	14 964.5	$^3T_1$(P 55%, F 45%)	$^3A_2$
	17	19 999.6 (obs)	$^1T_1$(G)	$^1A_2$
	18 – 23	22 887.5	$^3T_1$(F 70%, P 30%)	^3E
	24 – 26	23 680.1	$^3T_2$(F)	$^3B_2$
	27 – 29	25 132.8	$^3T_1$(F 55%, P 45%)	$^3A_2$

	30	26 746.2	$^1A_1$(G 75%, D 25%)	$^1A_1$
	31 – 32	28 837.0	$^1T_1$(G 80%, D 20%)	^1E
	33 – 38	29 700.7	$^3T_1$(P 60%, F 40%)	^3E
	39	29 818.3	$^1T_2$(D)	$^1B_2$
	40	31 410.2	^1E (G 65%, D 35%)	$^1B_1$
	41	33 080.4	$^1T_2$(G)	$^1B_2$
	42	35 567.8	^1E (G 50%, D 40%, S 10%)	$^1A_1$
	43 – 44	35 611.8	$^1T_2$(G 70%, D 30%)	^1E
	45	48 238.4	$^1A_1$(S 75%, G 25%)	$^1A_1$
d) $Cr(O^tBu)_4$				
Complex, model used	Term number	Relative energy [a]	Description in T_d (with free-ion parentage)[b]	Description in D_{2d}
calculated using AOM with ideal D_{2d} geometry with: B = 817.2, C = 3360.0. ε_σ = 6961.3	1 – 3	0.0	$^3A_2$(F)	$^3B_1$
	4 – 9	9040.1 (obs 8700)	$^3T_2$(F)	^3E
	10 – 12	9726.1 (obs 9500)	$^3T_2$(F)	$^3B_2$
	13	12 842.8	^1E (D 70%, G 30%)	$^1B_1$
	14	12 860.5	^1E (D 70%, G 30%)	$^1A_1$
	15 – 20	14 990.9	$^3T_1$(F 80%, P 20%)	^3E
	21 – 23	15 098.4 (obs 15 750)	$^3T_1$(F 80%, P 20%)	$^3A_2$
	24	21 302.9	$^1A_1$(G 90%, S 10%)	$^1A_1$
	25 – 26	21 585.4	$^1T_2$(D 80%, G 20%)	^1E
	27	22 180.9	$^1T_2$(D 80%, 20%)	$^1B_2$
	28 – 30	24 958.0 (obs)	$^3T_1$(P 85%, F 15%)	$^3A_2$
	31 – 36	25 077.2 (obs)	$^3T_1$(P 80%, F 20%)	^3E
	37 – 38	25 574.3	$^1T_1$(G)	^1E
	39	26 236.9	$^1T_1$(G)	$^1A_2$
	40	32 577.5	^1E (G 70%, D 30%)	$^1B_1$
	41	32 965.6	$^1T_2$(G 80%, D 20%)	$^1B_2$
	42	33 488.0	^1E (G 70%, D 30%)	$^1A_1$
	43 – 44	33 549.3	$^1T_2$(G 80%, D 20%)	^1E
	45	55 270.3	$^1A_1$(S 90%, G 10%)	$^1A_1$
e) $Cr(OSiMe^tBu_2)_4$ = $Cr(DTBMS)_4$, preferred model (Figure 5)				
Complex, model used	Term number	Relative energy [a]	Description in T_d (with free-ion parentage)[b]	Description in D_{2d}
calculated using AOM with ideal D_{2d} geometry with: B = 427.5,	1 – 3	0.0	$^3A_2$(F)	$^3B_1$
	4	7644.7	^1E (D 64%, G 36%)	$^1A_1$
	5	7703.3	^1E (D 66%, G 34%)	$^1B_1$
	6 – 11	8069.2 (obs)	$^3T_2$(F)	^3E
	12 – 14	9598.8 (obs)	$^3T_2$(F)	$^3B_2$

C = 2206.0. ε_σ = 6600.0. $\varepsilon_{\pi\text{-}c}$ = 230.0	15 – 20	12 498.7 (obs)	$^3T_1$(F 57%, P 43%)	^3E
	21 – 23	12 785.4	$^3T_1$(F 65%, P 35%)	$^3A_2$
	24	13 251.4	$^1A_1$(G 87%, S 13%)	$^1A_1$
	25 – 26	15 667.5	$^1T_2$(D 70%, G 30%)	^1E
	27	17 142.1	$^1T_2$(D 75%, G 25%)	$^1B_2$
	28 – 29	17 967.7	$^1T_1$(G)	^1E
	30	18 519.6 (obs)	$^1T_1$(G)	$^1A_2$
	31 – 33	19 083.6	$^3T_1$(P 65%, F 35%)	$^3A_2$
	34 – 39	19 851.1 [c]	$^3T_1$(P 56%, F 44%)	^3E
	40	24 867.1	^1E (G 66%, D 34%)	$^1B_1$
	41	25 027.0	$^1T_2$(G 75%, D 25%)	$^1B_2$
	42 – 43	26 004.7	$^1T_2$(G 90%, D 10%)	^1E
	44	26 186.8	^1E (G 65%, D 35%)	$^1A_1$
	45	38 452.8	$^1A_1$(S 87%, G 13%)	$^1A_1$
f) $Cr(OSiMe^tBu_2)_4$ = $Cr(DTBMS)_4$, disfavored model (Figure S1)				
calculated using AOM with ideal D_{2d} geometry with: B = 868.4, C = 3352.5, ε_σ = 6961.3, $\varepsilon_{\pi\text{-}s}$ = 1403.5	1 – 3	0.0	$^3A_2$(F)	$^3B_1$
	4 – 6	5683.5	$^3T_2$(F)	$^3B_2$
	7 – 12	8053.7 (obs)	$^3T_2$(F)	^3E
	13	11 823.9	^1E (D 65%, G 35%)	$^1A_1$
	14 – 19	12 511.7 (obs)	$^3T_1$(F 90%, P 10%)	^3E
	20	13 103.8	^1E (D 75%, G 25%)	$^1B_1$
	21 – 23	13 486.4	$^3T_1$(F 95%, P 5%)	$^3A_2$
	24	18 519.5 (obs)	$^1T_2$(D 80%, G 20%)	$^1B_2$
	25 – 26	20 358.4	$^1T_2$(D 70%, G 30%)	^1E
	27	22 529.4	$^1A_1$(G 85%, D 10%, S 5%)	$^1A_1$
	28 – 33	22 692.7 (obs)[c]	$^3T_1$(P 90%, F 10%)	^3E
	34 – 36	24 147.6	$^3T_1$(P 95%, F 5%)	$^3A_2$
	37 – 38	24 405.1	$^1T_1$(G 80%, D 20%)	^1E
	39	26 647.5	$^1T_1$(G)	$^1A_2$
	40	30 155.3	^1E (G 75%, D 25%)	$^1B_1$
	41	30 278.9	^1E (G 75%, D 25%)	$^1A_1$
	42	30 423.1	$^1T_2$(D 80%, G 20%)	$^1B_2$
	43 – 44	30767.1	$^1T_2$(G 90%, D 10%)	^1E
	45	53 530.3	$^1A_1$(S 95%, G 5%)	$^1A_1$

[a] The observed bands are also indicated. If no value is given, then the match is exact within a few cm^{-1} (< 100 cm^{-1}); otherwise, the observed value is given in parentheses.

[b] If no percentage is given, then it is essentially 100% of that free-ion term. These values among all terms do not always add up to 100% for a given free-ion due to the extensive rounding used. This information is provided mainly as an indication of how mixed the free-ion terms in such a strong ligand field are.

[c] Strong absorption bands begin at roughly 22 200 cm^{-1} ($\lambda \geq 450$ nm), but may be primarily the tail of CT band(s) that extend well into the UV region.

Table S5. Edited LFT output using the program Ligfield to show the effect of SOC on the energy levels of selected CrL_4 complexes.

a) $Cr(Nor)_4$

These matrices were generated from the following terms: ^3P ^3F ^1S ^1D ^1G of d^2 in SLM_SM_L-basis.
One electron parametrization was taken from: AOM. The AOM-matrices were not barycentered.

Ligator	Theta	Phi	Psi	Parameter	Value (cm^{-1})	Parameter	Value (cm^{-1})
C1	54.7356	45	0	εσ	12097.5	Racah *B*	409.87
C2	125.2644	135	0	εσ	12097.5	Racah *C*	1684.60
C1'	54.7356	225	0	εσ	12097.5	Spin-orbit coupling	180.00
C2'	125.2644	-45	0	εσ	12097.5		

			Symmetry of eigenfunctions			**Orbital populations** theta	ksi	eta	zeta	epsilon
Function	Energy	2*S*+1	*O**	D_4*	D_2*	z^2	*yz*	*xz*	*xy*	x^2-y^2
1	0.00	2.99987	T_2	--	--	0.999827	0.000105	0.000126	0.000085	0.999858
2	0.00	2.99987	T_2	--	--	0.999858	0.000126	0.000064	0.000126	0.999827
3	0.00	2.99987	T_2	--	--	0.999842	0.000085	0.000126	0.000105	0.999843
4	6583.10	1.00163	E	B_1	A_1	0.997714	0.002115	0.002115	0.000364	0.997691
5	6583.10	1.00163	E	A_1	A_1	0.997691	0.000948	0.000948	0.002699	0.997714
6	12242.49	1.00207	A_1	A_1	A_1	0.971072	0.019285	0.019285	0.019285	0.971072
7	16045.47	3.00000	A_2	B_1	A_1	0.5	0.333333	0.333333	0.333333	0.5
8	16087.99	2.99954	T_2	--	--	0.270939	0.451501	0.499819	0.048681	0.729060
9	16087.99	2.99954	T_2	--	--	0.633911	0.496995	0.003260	0.499745	0.366088
10	16087.99	2.99954	T_2	--	--	0.595148	0.051505	0.496922	0.451574	0.404851
11	16174.99	2.99886	E	A_1	A_1	0.268901	0.499403	0.499403	0.001074	0.731219
12	16174.99	2.99886	E	B_1	A_1	0.731219	0.167184	0.167183	0.665513	0.268901
13	16175.50	2.99966	T_1	--	--	0.303516	0.450189	0.499833	0.050118	0.696345
14	16175.50	2.99966	T_1	--	--	0.615281	0.499780	0.000626	0.499734	0.384580
15	16175.50	2.99966	T_1	--	--	0.580994	0.050171	0.499681	0.450287	0.418866
16	20573.90	2.99777	A_1	A_1	A_1	0.485728	0.342848	0.342848	0.342848	0.485728
17	20577.86	2.99895	T_1	--	--	0.692517	0.481447	0.499731	0.050881	0.275424
18	20577.86	2.99895	T_1	--	--	0.374351	0.454208	0.079747	0.498104	0.593590
19	20577.86	2.99895	T_1	--	--	0.385043	0.096404	0.452581	0.483074	0.582897
20	20591.02	2.99730	T_2	--	--	0.725236	0.480654	0.499351	0.057697	0.237062
21	20591.02	2.99730	T_2	--	--	0.352609	0.470577	0.069452	0.497673	0.609689
22	20591.02	2.99730	T_2	--	--	0.365602	0.086472	0.468899	0.482332	0.596696
23	20599.16	2.99911	E	B_1	A_1	0.741697	0.499398	0.499398	0.038883	0.220624
24	20599.16	2.99911	E	A_1	A_1	0.220624	0.192388	0.192388	0.652903	0.741697

25	22662.27	1.00404	T_2	--	--	0.250326	0.700458	0.296323	0.011140	0.741753
26	22662.27	1.00404	T_2	--	--	0.248880	0.295239	0.703452	0.009229	0.743199
27	22662.27	1.00404	T_2	--	--	0.988912	0.012223	0.008146	0.987552	0.003167
28	24425.15	1.00167	T_1	--	--	0.744874	0.762213	0.230800	0.007049	0.255065
29	24425.15	1.00167	T_1	--	--	0.748548	0.22907	0.768837	0.002154	0.251391
30	24425.15	1.00167	T_1	--	--	0.006486	0.008778	0.000424	0.990859	0.993452
31	33914.44	2.99960	E	A_1	A_1	0.010886	0.807769	0.807769	0.346174	0.027403
32	33914.44	2.99960	E	B_1	A_1	0.027403	0.500039	0.500039	0.961633	0.010886
33	33915.89	2.99796	T_2	--	--	0.015162	0.844677	0.614397	0.502294	0.023469
34	33915.89	2.99796	T_2	--	--	0.015116	0.613721	0.847035	0.500613	0.023515
35	33915.89	2.99796	T_2	--	--	0.027669	0.502971	0.499936	0.958462	0.010962
36	34019.07	2.99971	T_1	--	--	0.011635	0.859936	0.605140	0.502665	0.020625
37	34019.07	2.99971	T_1	--	--	0.011583	0.604187	0.862666	0.500888	0.020677
38	34019.07	2.99971	T_1	--	--	0.025171	0.503618	0.499935	0.964188	0.007088
39	34065.46	2.99921	A_1	A_1	A_1	0.014616	0.656923	0.656923	0.656923	0.014616
40	39389.91	1.00079	E	B_1	A_1	0.001967	0.997930	0.997930	0.000274	0.001898
41	39389.91	1.00079	E	A_1	A_1	0.001898	0.332826	0.332826	1.330483	0.001967
42	39449.90	1.00128	T_2	--	--	0.007171	0.969520	0.992530	0.030642	0.000138
43	39449.90	1.00128	T_2	--	--	0.001848	0.860023	0.142926	0.989742	0.005461
44	39449.90	1.00128	T_2	--	--	0.001945	0.163148	0.857236	0.972307	0.005364
45	49125.06	1.00095	A_1	A_1	A_1	0.028584	0.647611	0.647611	0.647611	0.028584

b) $Cr(OSiMe^tBu_2)_4$ = $Cr(DTBMS)_4$ (favored model; Figure 5)

These matrices were generated from the following terms: ^3P ^3F ^1S ^1D ^1G of d^2 in SLM_SM_L-basis.
One electron parametrization was taken from: AOM. The AOM-matrices were not barycentered.

Ligator	Theta	Phi	Psi	Parameter	Value (cm^{-1})	Parameter	Value (cm^{-1})
O1	56.11	45	0	εσ	6600.0	επ–c	230.0
O2	123.89	135	0	εσ	6600.0	επ–c	230.0
O1'	56.11	225	0	εσ	6600.0	επ–c	230.0
O2'	123.89	-45	0	εσ	6600.0	επ–c	230.0

Parameter	Value (cm^{-1})
Racah *B*	427.50
Racah *C*	2206.00
Spin-orbit coupling	198.00

				Symmetry of eigenfunctions			**Orbital** theta	**populations** ksi	eta	zeta	epsilon
Function	Energy	2*S*+1	M_S	*O**	D_4*	D_2*	z^2	*yz*	*xz*	*xy*	x^2-y^2
1	0	2.99973	0	T_2	B_2	B_1	0.999054	0.000613	0.000613	0.000134	0.999586
2,3 (2)	0.565	2.99968	±0.99923	--	E	--	0.999410	0.000386	0.000386	0.000434	0.999384
	(*D* =	+0.565	cm^{-1})								
4	7542.37	1.30224	0	--	A_1	A_1	0.707961	0.079020	0.079020	0.006497	1.127502
5	7619.83	1.29059	0	--	B_1	A_1	0.868843	0.075458	0.075458	0.008253	0.971988
6	8017.50	2.99940	0	T_2	B_2	B_1	0.184683	0.499457	0.499457	0.001396	0.815007
7	8069.88	2.73948	0	--	B_1	A_1	0.310207	0.432614	0.432614	0.007085	0.817480
8,9 (2)	8076.24	2.99949	±0.00017	--	E	--	0.205172	0.499340	0.499340	0.001488	0.794660
10	8137.22	2.99972	0	T_1	A_2	B_1	0.224158	0.499931	0.499931	0.000215	0.775764
11	8228.32	2.70233	0	--	A_1	A_1	0.297607	0.426670	0.426670	0.000999	0.848055
12,13 (2)	9603.96	2.99939	±0.99637	--	E	--	0.997175	0.001817	0.001817	0.997019	0.002172
14	9618.86	2.97433	0	--	B_1	A_1	0.994513	0.003210	0.003210	0.982780	0.016288
15	12468.06	2.87606	0	--	A_1	A_1	0.671814	0.470734	0.470734	0.133900	0.252818
16	12488.17	2.99975	0	T_2	B_2	B_1	0.702388	0.500010	0.500010	0.151306	0.146287
17,18 (2)	12502.46	2.99959	±0.03550	--	E	--	0.656174	0.490857	0.490857	0.166517	0.195594
19	12507.92	2.99460	0	--	B_1	A_1	0.704313	0.496619	0.496619	0.154605	0.147843
20	12535.65	2.99929	0	T_1	A_2	B_1	0.672099	0.499823	0.499823	0.130691	0.197564
21	12773.74	2.84999	0	--	A_1	A_1	0.106497	0.199198	0.199198	0.731361	0.763747
22,23 (2)	12810.15	2.99912	±0.96074	--	E	--	0.032774	0.217881	0.217881	0.765790	0.765674
24	13361.02	1.26845	0	--	A_1	A_1	1.007093	0.108054	0.108054	0.111701	0.665098
25,26 (2)	15661.32	1.01261	±0.00307	--	E	--	0.152978	0.500988	0.500988	0.023668	0.821378
27	17124.97	1.02465	0	T_2	B_2	B_1	0.951716	0.042788	0.042788	0.961744	0.000965

28, 29 (2)	17975.57	1.01610	±0.00678	--	E	--	0.832294	0.500674	0.500674	0.003700	0.162658
30	18526.72	1.01359	0	T_1	A_2	B_1	0.001253	0.003398	0.003398	0.997746	0.994204
31	19100.40	2.99955	0	--	A_1	A_1	0.000786	0.790488	0.790488	0.209296	0.208942
32, 33 (2)	19116.43	2.97980	±0.98923	--	E	--	0.009915	0.788382	0.788382	0.206628	0.206694
34	19858.97	2.99981	0	--	B_1	A_1	0.114367	0.499842	0.499842	0.847071	0.038878
35	19877.13	2.99940	0	--	A_1	A_1	0.103158	0.499674	0.499674	0.869991	0.027503
36,37 (2)	19877.63	2.99288	±0.00029	--	E	--	0.108149	0.499705	0.499705	0.855988	0.036453
38	19885.26	2.97481	0	T_2	B_2	B_1	0.125600	0.493714	0.493714	0.848836	0.038136
39	19886.41	2.98739	0	T_1	A_2	B_1	0.102490	0.496847	0.496847	0.871348	0.032468
40	24886.24	1.00118	0	E	B_1	A_1	0.007757	0.992257	0.992257	0.000206	0.007522
41	25045.79	1.00166	0	T_2	B_2	B_1	0.036560	0.963419	0.963419	0.036584	0.000019
42, 43 (2)	26023.38	1.00136	±0.00014	--	E	--	0.005959	0.499970	0.499970	0.978768	0.015333
44	26205.44	1.00097	0	--	A_1	A_1	0.001336	0.395371	0.395371	1.192814	0.015107
45	38475.12	1.00102	0	--	A_1	A_1	0.103748	0.530791	0.530791	0.743441	0.091228

III. QCT Calculations of CrL_4 complexes: QTAIM analysis.

Quantum Theory of Atoms-in-Molecules (QTAIM)[40] topological analysis of electron density is a powerful tool for chemical bonding and structure analysis in molecules and crystals. The first derivative (gradient) of the electron density vanishes at its ''critical points'' (CP) such as maxima, minima, and saddle points.

Atom positions are determined by electron density maxima. QTAIM atomic charges and volumes are obtained using the electron density integrated over atomic basins (up to 0.001 e/Bohr^3 level).

In an equilibrium geometry, a pair of bonded atoms are linked by a line, i.e., a bond path, along which the electron density is maximally concentrated ("ridges" of electron density). The presence of a bond path between two atoms is the necessary condition for the presence of a chemical bond. The set of bond paths for a given molecule, the molecular graph, faithfully recovers the network of chemical bonds that are assigned on the basis of chemical considerations. The saddle point of electron density at the bond path is a bond critical point (BCP; also called a line critical point, LCP). QTAIM bond characteristics are evaluated in terms of electron density, ρ, its Laplacian, $\nabla^2\rho$, given by Eqn S1:

$$\nabla^2\rho = \lambda_1 + \lambda_2 + \lambda_3 \qquad \text{(S1)}$$

and the bond ellipticity, ε, given by Eqn S2:

$$\varepsilon = \frac{\lambda_1}{\lambda_2} - 1 \qquad \text{(S2)}$$

each calculated at BCPs, which are defined by the λ_i eigenvalues of the Hessian of the BCP electron density, $\lambda_1 < \lambda_2 < 0 < \lambda_3$. The BCP electron density, ρ_{BCP}, is proportional to the bond strength; the value and sign of its BCP Laplacian, $\nabla^2\rho_{BCP}$, describes the relative electron density

contribution of the bonded atoms to the bond (covalent *vs.* dative bonding) and its magnitude is a measure of an electron density transfer between bonded atoms; its BCP bond ellipticity, ε_{BCP}, describes its deviation from cylindrical symmetry (such as in ideal single or triple bonds) due to its double-bond character, mechanical strain, and other perturbations. The electron delocalization index, DI(A,B), is the average number of electrons delocalized (shared) between atoms A and B. For atoms A and B that are connected by a bond path it corresponds to a bond index (order).

Ring critical points (RCP) are located inside cyclic structures with two positive and one negative eigenvalues of the Hessian of the RCP electron density. Local minima of electron density are known as cage critical points (CCP) with three positive eigenvalues of the Hessian of the CCP electron density. QTAIM analysis was performed in the AIMAll package[41] using the wave function from the Gaussian09 wfn file.

Positive Cr charges decrease in the sequence fluoride > siloxides > alkoxides > amides > alkyls, see Table S6. Alkyls have the greatest atomic volumes, followed by the amides see Table S6. These trends indicate higher stability of siloxides in comparison with alkoxides. The highest α-spin populations at Cr atoms may be ascribed to alkyls and $Cr(NMeCH^tBu_2)_4$ (over two electrons) whereas the lowest ones to siloxides and CrF_4, see Table S6. This implies relevant negative spin density at alkyl and $NMeCH^tBu_2$ ligands and relevant positive spin density at fluorido, alkoxido, and siloxido ligands.

Table S6. QTAIM electron densities, ρ_{BCP}, their Laplacians, $\nabla^2\rho_{BCP}$, (both in [e/bohr^3]) and bond ellipticities, ε_{BCP}, at bond critical points, BCP, and delocalization indices, DI, of Cr-X bonds in the UB3LYP/6-311G* optimized tetracoordinated neutral Cr^{IV} complexes in triplet spin states.

Compound	X	ρ_{BCP}(Cr-X)	$\nabla^2\rho_{BCP}$(Cr-X)	ε_{BCP}(Cr-X)	DI(Cr,X)
CrF_4	F	0.1673	0.8735	0.001	0.948
		0.1673	0.8735	0.001	0.948
		0.1673	0.8733	0.001	0.948
		0.1673	0.8735	0.001	0.948
CrF_4 (Evaluated in 6-311+G* basis set)	F	0.1738	0.9155	0.000	0.946
		0.1737	0.9150	0.000	0.946
		0.1735	0.9138	0.001	0.945
		0.1740	0.9164	0.001	0.946
Alkyl complexes					
$Cr(CH_2SiMe_3)_4$	C	0.1192	0.0850	0.025	0.885
		0.1187	0.0858	0.023	0.883
		0.1186	0.0886	0.025	0.883
		0.1188	0.0884	0.026	0.884
Cr^tBu_4	C	0.1013	0.0602	0.001	0.765
		0.1014	0.0602	0.001	0.766
		0.1013	0.0602	0.002	0.766
		0.1012	0.0602	0.000	0.766
Amido complexes					
$Cr(NMeCH^tBu_2)_4$	N	0.1064	0.3535	0.132	0.796
		0.1089	0.3677	0.140	0.819
		0.1118	0.3649	0.144	0.835
		0.1127	0.3669	0.143	0.837
$Cr(NMe_2)_4$	N	0.1426	0.4134	0.161	0.921
		0.1424	0.4137	0.163	0.920
		0.1425	0.4120	0.162	0.920
		0.1425	0.4122	0.162	0.921
Alkoxido complexes					
$Cr(OCH^tBu_2)_4$	O	0.1482	0.6661	0.008	0.904
		0.1482	0.6660	0.008	0.904
		0.1482	0.6661	0.008	0.904
		0.1482	0.6660	0.008	0.904
$Cr(O^tBu)_4$	O	0.1565	0.6526	0.069	0.922
		0.1565	0.6528	0.069	0.922
		0.1564	0.6525	0.069	0.922
		0.1564	0.6524	0.069	0.922

$Cr(OMe)_4$	O	0.1661 0.1620 0.1622 0.1576	0.6487 0.6481 0.6554 0.6433	0.055 0.040 0.077 0.086	0.960 0.938 0.921 0.931
Siloxido complexes					
$Cr(DTBMS)_4$	O	0.1516 0.1515 0.1516 0.1515	0.6784 0.6783 0.6779 0.6774	0.021 0.021 0.021 0.021	0.917 0.913 0.916 0.916
$Cr(OSiMe_3)_4$	O	0.1586 0.1586 0.1586 0.1586	0.6860 0.6859 0.6860 0.6859	0.027 0.027 0.027 0.027	0.932 0.932 0.932 0.932

Table S7. QTAIM atomic charges, q, atomic volumes, V, and excess α-spin populations, N_α of Cr atoms in the UB3LYP/6-311G* optimized neutral tetracoordinated Cr^{IV} complexes in triplet spin state.

Compound	q(Cr)	V(Cr) [$bohr^3$	N_α(Cr)	CSD or local code
CrF_4	2.09	59.0	1.79	
CrF_4 [a]	2.09	63.3	1.80	
Alkyl complexes				
$Cr(CH_2SiMe_3)_4$	1.44	73.3	2.29	CrCH2SiMe34
Cr^tBu_4	1.33	80.8	2.66	CrCMe34
Amido complexes				
$Cr(NMeCH^tBu_2)_4$	1.67	68.4	2.44	NMeLIBCRB
$Cr(NMe_2)_4$	1.71	64.9	1.93	CrNMe24
Alkoxido complexes				
$Cr(OCH^tBu_2)_4$	1.93	62.6	1.84	LIBCRB
$Cr(O^tBu)_4$	1.91	60.2	1.84	MetALUHOF
$Cr(OMe)_4$	1.90	62.9	1.85	CrOMe4
Siloxido complexes				
$Cr(OSiMe^tBu_2)_4$	2.02	62.3	1.77	SESROZ
$Cr(OSiMe_3)_4$	2.00	61.1	1.78	Met SESROZ

[a] Evaluated in 6-311+G* basis.

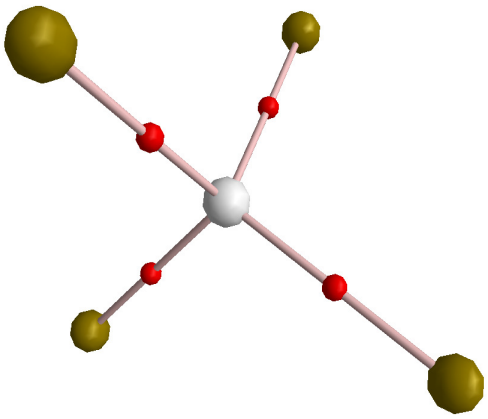

Figure S2. QTAIM molecular graph of CrF_4 in triplet spin state (white – Cr, dark yellow – F, red – bond critical point (BCP)).

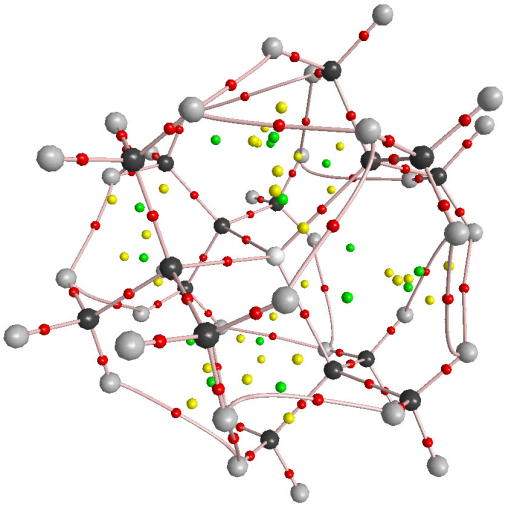

Figure S3. QTAIM molecular graph of Cr^tBu_4 in triplet spin state (white – Cr, black – C, gray - H, red – bond critical point, yellow – ring critical point (RCP), green – cage critical point (CCP)).

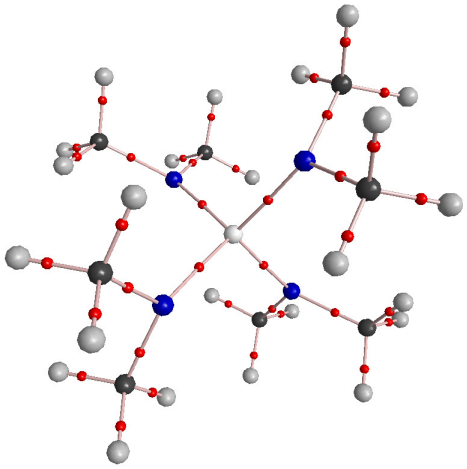

Figure S4. QTAIM molecular graph of $Cr(NMe_2)_4$ in triplet spin state (white – Cr, black – C, gray - H, blue – N, red – bond critical point).

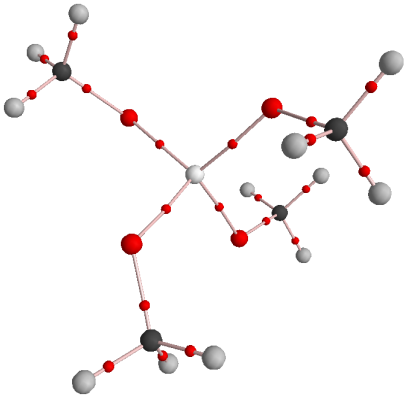

Figure S5. QTAIM molecular graph of $Cr(OMe)_4$ in triplet spin state (white – Cr, black – C, gray - H, large red – O, small red – bond critical point).

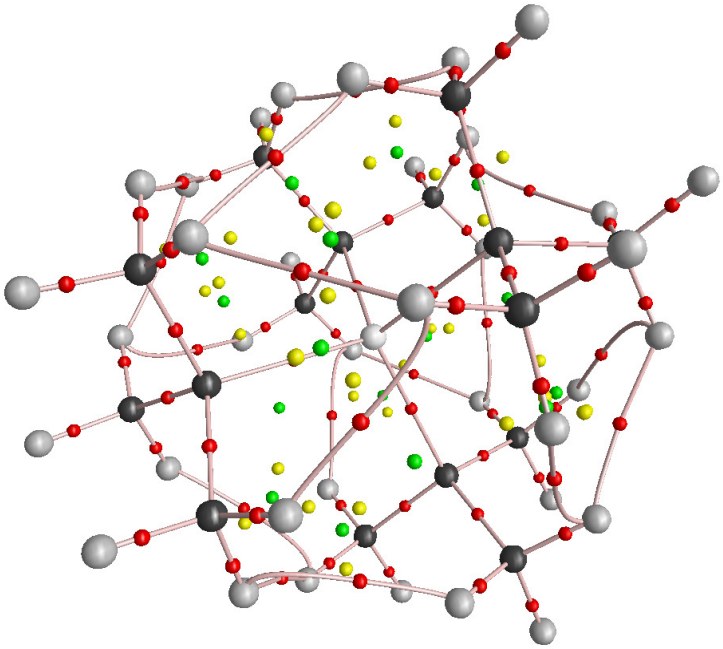

Figure S6. QTAIM molecular graph of $Cr(O^tBu)_4$ in triplet spin state (white – Cr, black – C, gray - H, large red – O, small red – bond critical point, yellow – ring critical point (RCP), green – cage critical point (CCP)).

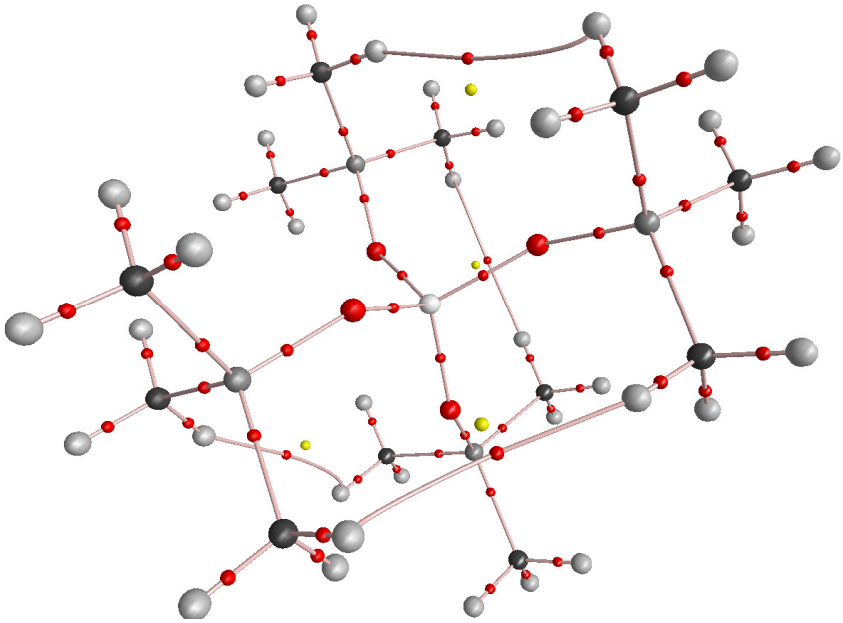

Figure S7. QTAIM molecular graph of $Cr(OSiMe_3)_4$ in triplet spin state (white – Cr, black – C, gray - H, dark gray – Si, big red – O, small red – bond critical point (BCP), yellow – ring critical point (RCP)).

IV. QCT Calculations of CrL_4 complexes: Energetics and electronic structure

Table S8. Spin squares ($\langle S^2 \rangle$), DFT energies (E_{DFT}) and Gibbs free energies (energies in hartree) at 298 K (G_{298}) of B3LYP/6-311G* optimized structures of neutral CrL_4 complexes in singlet and triplet spin states (preferred state in bold). The structural provenance (CSD code) is given where applicable.

Compound	M_S	Formalism	$\langle S^2 \rangle$	E_{DFT}	G_{298}
CrF_4 [b]	1	unrestricted	1.001	-1444.06708	-1444.08821
(6-311+G* basis set)		restricted	-	-1444.06638	-1444.08804
	3	unrestricted	2.012	**-1444.12961**	**-1444.15198**
Alkyls					
$Cr(CH_2SiMe_3)_4$	1	unrestricted	1.002	-2838.98488	-2838.50891
(from SESROZ)		restricted	-	-2838.94263	-2838.46745
	3	unrestricted	2.109	**-2839.01052**	-2838.53780
Cr^tBu_4	1	unrestricted	1.004	-1675.89103	-1675.45349
		restricted	-	-1675.84652	-1675.41164
	3	unrestricted	2.292	**-1675.91943**	**-1675.48448**
Amidos					
$Cr(NMeCH^tBu_2)_4$	1	unrestricted	0.711	-2840.96526	-2839.80630
(from LIBCRB)		restricted	-	-2840.95924	-2839.80031
	3	unrestricted	2.254	**-2840.98112**	**-2839.82681**
$Cr(N^tBu_2)_4$	1	unrestricted		unstable	
		restricted	-	-2526.22706	-2525.27862
	3	unrestricted		unstable	
$Cr(NMe_2)_4$	1	unrestricted	0.439	-1582.89494	-1582.61308
		restricted	-	-1582.89280	-1582.61007
	3	unrestricted	2.036	**-1582.90292**	**-1582.62516**
Alkoxides					
$Cr(OCH^tBu_2)_4$	1	unrestricted	1.002	-2763.42081	-2762.42982
(from LIBCRB)		restricted	-	-2763.39720	-2762.40375
	3	unrestricted	2.023	**-2763.44028**	**-2762.45322**
$Cr(O^tBu)_4$	1	unrestricted	0.940	-1977.09553	-1976.65369
(from ALUHOF)		restricted	-	-1977.07454	-1976.63166
	3	unrestricted	2.021	**-1977.11353**	**-1976.66890**
$Cr(OMe)_4$	1	unrestricted	0.904	-1505.17886	-1505.05608
		restricted	-	-1505.16142	-1505.03616
	3	unrestricted	2.022	**-1505.19340**	**-1505.07314**
Siloxides					
$Cr(OSiMe^tBu_2)_4$	1	unrestricted	1.001	-3926.65542	-3925.60410
= $Cr(DTBMS)_4$		restricted	-	-3926.61813	-3925.56846
(from SESROZ)	3	unrestricted	2.003	**-3926.67493**	**-3925.62382**
$Cr(OSiMe_3)_4$	1	unrestricted	0.997	-2983.04109	-2982.65681
(from SESROZ)		restricted	-	-2983.00669	-2982.61888
	3	unrestricted	2.014	**-2983.06077**	**-2982.68127**

Table S9. BLYP/6-311G* d-orbital and localized orbital populations of Cr-L bonds for the central Cr atom.

	$^3[Cr^tBu_4]$	$^3[Cr(NMe_2)_4]$	$^1[Cr(NMe_2)_4]$	$^3[Cr(OMe)_4]$	$^3[CrF_4]$
$d_{z2}(\alpha)$	0.948	0.837	0.348	0.906	1.012
$d_{xz}(\alpha)$	0.484	0.359	0.322	0.435	0.310
$d_{yz}(\alpha)$	0.484	0.564	0.323	0.374	0.310
$d_{x2y2}(\alpha)$	0.948	0.908	0.915	0.956	1.012
$d_{xy}(\alpha)$	0.484	0.366	0.258	0.345	0.310
$d_{z2}(\beta)$	0.017	0.196	0.347	0.197	0.182
$d_{xz}(\beta)$	0.305	0.292	0.322	0.254	0.265
$d_{yz}(\beta)$	0.305	0.231	0.323	0.275	0.265
$d_{x2y2}(\beta)$	0.017	0.172	0.915	0.176	0.182
$d_{xy}(\beta)$	0.305	0.290	0.258	0.282	0.265
LOCσ(Cr-L)	0.628	0.359	0.435	0.421	0.409
LOCπ(Cr-L)		0.240	0.202	0.146	0.075
	$^3[Cr(O^tBu)_4]$	$^3[Cr(OSiMe_3)_4]$		$^3[Cr(NMeCH^tBu_2)_4]$	$^3[Cr(NMeCH^tBu_2)_4]$
$d_{z2}(\alpha)$	0.994	0.980		0.949	0.832
$d_{xz}(\alpha)$	0.335	0.313		0.377	0.288
$d_{yz}(\alpha)$	0.335	0.340		0.386	0.278
$d_{x2y2}(\alpha)$	0.920	0.991		0.945	0.385
$d_{xy}(\alpha)$	0.410	0.313		0.525	0.353
$d_{z2}(\beta)$	0.206	0.180		0.049	0.775
$d_{xz}(\beta)$	0.273	0.263		0.266	0.292
$d_{yz}(\beta)$	0.273	0.263		0.269	0.277
$d_{x2y2}(\beta)$	0.162	0.188		0.133	0.441
$d_{xy}(\beta)$	0.261	0.263		0.262	0.332
LOCσ(Cr-L)	0.385	0.360		0.320	0.325
LOCπ(Cr-L)	0.140	0.117		0.225	0.250
	$^3[Cr(OCH^tBu_2)_4]$	$^3[Cr(OSiMe^tBu_2)_4]$ ExpGeom	$^3[Cr(OSiMe^tBu_2)_4]$ OptGeom	$^3[Cr(CH_2SiMe_3)_4]$	
$d_{z2}(\alpha)$	0.990	0.980	0.980	0.953	
$d_{xz}(\alpha)$	0.348	0.328	0.328	0.436	
$d_{yz}(\alpha)$	0.348	0.310	0.310	0.438	
$d_{x2y2}(\alpha)$	0.799	0.991	0.991	0.952	
$d_{xy}(\alpha)$	0.498	0.310	0.310	0.441	
$d_{z2}(\beta)$	0.185	0.187	0.187	0.032	
$d_{xz}(\beta)$	0.283	0.253	0.253	0.313	
$d_{yz}(\beta)$	0.283	0.259	0.259	0.316	
$d_{x2y2}(\beta)$	0.219	0.191	0.191	0.050	
$d_{xy}(\beta)$	0.192	0.259	0.259	0.316	
LOCσ(Cr-L)	0.343	0.330	0.295	0.600	
LOCπ(Cr-L)	0.158	0.117	0.119		

Table S10. Total energies (in hartree; calculated using 6-311G* basis set) from BLYP and state averaged CASSCF(2,5) calculations of triplet and singlet states of selected neutral CrL_4 complexes, using the particular B3LYP/6-311G* optimized structures (the preferred state is given in **bold**).

	BLYP		CASSCF(2,5)	
	triplet	singlet	triplet	singlet
Cr^tBu_4	**-1675.5237**	-1675.4554	**-1669.8820**	-1669.8160
$Cr(NMe_2)_4$	-1582.3542 (-1582.6575)[a]	**-1582.6681**	**-1577.7837** (-1577.8298)[a]	-1577.7811
$Cr(OMe)_4$	**-1505.1045**	-1505.0911	**-1501.1342**	-1501.0702
$Cr(OSiMe_3)_4$	**-2982.6251**	-2982.6022	**-2974.3038**	-2974.2349
$Cr(O^tBu)_4$	**-1976.6968**	-1976.6811	**-1969.6874**	-1969.6225
$Cr(NMeCH^tBu_2)_4$	**-2839.8686**	-2839.8551	**-2826.8839**	-2826.8254

[a] C_2 symmetry restricted geometry.

Table S11. Energies (in hartree; calculated using 6-311G* basis set) of lowest triplet and singlet state roots of selected CrL_4 complexes from CASSCF(2,5) and NEVPT2 calculations based on either triplet or singlet reference state, where rootT and rootS denote the lowest triplet and singlet state, respectively (the preferred state is given in **bold**).

	Cr^tBu_4		$Cr(NMe_2)_4$		$Cr(OMe)_4$	
	triplet	singlet	triplet	singlet	triplet	singlet
CASSSF-rootT	**-1669.9705**	**-1669.9667**	**-1577.9325** (-1577.9121)[a]	**-1577.9290**	**-1501.2243**	**-1501.2237**
CASSSF-rootS	-1669.8991	-1669.8991	-1577.8712 (-1577.8691)[a]	-1577.8911	-1501.1576	-1501.1643
NEVPT2-rootT	**-1672.8736**	**-1672.8920**	**1580.2964** (-1580.2544)[a]	-1580.2861	**-1503.0429**	**-1503.0598**
NEVPT2-rootS	-1672.8156	-1672.8362	-1580.2426 (-1580.2391)[a]	**-1580.3001**	-1502.9872	-1503.0199

[a] C_2 symmetry restricted geometry.

Table S12. CASSCF(2,5)/6-311G* and NEVPT2/6-311G* electronic d-d triplet transitions in the active space for selected CrL_4 complexes (all values in cm^{-1}).

CASSCF					
CrF_4	CrF_4 [a]	Cr^tBu_4	$Cr(NMe_2)_4$	$Cr(OMe)_4$	$Cr(DTBMS)_4$
11 842	11 596	12 653	11115	11 583	9 998
11 860	11 613	12 657	15044	13 612	10 148
11 865	11 619	12 675	15060	13 892	11 590
18 757	18 467	19 770	19726	18 218	17 006
18 798	18 506	19 774	21256	21 004	17 075
18 834	18 541	19 798	21274	22 185	17 154
31 006	30 691	32 281	32233	29 561	28 380
31 029	30 714	32 299	32249	32 772	28 638
31 053	30 737	32 323	34437	35 005	28 890
NEVPT2					
	CrF_4 [a]			$Cr(OMe)_4$	
	13 466			13 963	
	13 532			16 879	
	13 543			17 327	
	20 515			20 998	
	20 595			24 216	
	20 605			25 453	
	30 415			31 078	
	30 455			35 182	
	30 496			37 053	

[a] 6-311+G* basis set.

Table S13a. BLYP/6-311G* UNOs occupation numbers (occ), including MO eigenvalues (eval), showing the metal and ligand percentage of each orbital and the T_d -like symmetry label for ^{3}[Cr(DTBMS)$_4$], ^{3}[Cr^{t}Bu$_4$], and ^{3}[CrF$_4$].

#	^{3}[Cr(DTBMS)$_4$]	eval	occ	Cr(4s)	Cr(d_{z2})	Cr(d_{xz})	Cr(d_{yz})	Cr(d_{x2y2})	Cr(d_{xy})	O_1	O_2	O_3	O_4	T_d
199	HOMO-7	-0.2319	1.9999	14.9	0.5	0	0	0	0	18.9	18.6	18.9	18.6	A_1
200	HOMO-6	-0.2316	1.9999	0	0.1	0	0	14.6	1.9	18.8	16.4	18.7	16.4	E
201	HOMO-5	-0.2191	1.9999	0.3	18.3	0	0	0.1	0	17.0	17.2	17.0	17.2	E
202	HOMO-4	-0.2160	1.9982	0	0	0	0	3	22.9	12.1	12.1	12.1	12.1	T_2
203	HOMO-3	-0.2139	1.9980	0	0	9.7	14.8	0	0	5.0	20.0	4.9	20.0	T_2
204	HOMO-2	-0.2128	1.9980	0	0	14.9	9.9	0	0	20.7	4.6	20.7	4.6	T_2
205	HOMO-1	-0.1712	1.0000	0	77.5	0	0	3.2	0.1	3.8	3.6	3.8	3.7	E
206	HOMO	-0.1656	1.0000	0	3.2	0	0	76	2.9	3.3	3.2	3.3	3.2	E
207	LUMO	-0.1095	0.0020	0	0	43.3	29.7	0	0	8.7	2.1	8.8	2.1	T_2
208	LUMO+1	-0.1088	0.0020	0	0	29.8	43.4	0	0	2.0	8.6	2.0	8.6	T_2
209	LUMO+2	-0.1042	0.0018	0	0	0	0	2.6	70.3	5.1	5.0	5.2	5.0	T_2
210	LUMO+3	-0.0027	0.0001	2.6	49.3	0	0	0.1	0	2.4	2.4	2.4	2.4	E
211	LUMO+4	0.0121	0.0001	0.2	0.1	0	0	40.2	2.6	4.0	3.5	4.0	3.5	E
212	LUMO+5	0.0181	0.0001	87.2	1.8	0	0	0	0	-3	-3.3	-2.9	-3.2	A_1
#	^{3}[Cr^{t}Bu$_4$]	eval	occ	Cr(4s)	Cr(d_{z2})	Cr(d_{xz})	Cr(d_{yz})	Cr(d_{x2y2})	Cr(d_{xy})	C_1	C_2	C_3	C_4	T_d
73	HOMO-5	-0.2071	1.9992	20.5	0	0	0	0	0	16.0	16.0	16.1	16.2	A_1
74	HOMO-4	-0.2025	1.9823	0	0	1	31.3	0	7.3	4.1	22.9	14	1.0	T_2
75	HOMO-3	-0.2025	1.9822	0	0	38.3	0.5	0	0.9	11	5.6	16	9,4	T_2
76	HOMO-2	-0.2025	1.9822	0	0	0.3	7.8	0	31.5	16.5	3.0	1.4	21.2	T_2
77	HOMO-1	-0.1659	1.0000	0	57.7	0	0	36.3	0	0.2	0.2	0.2	0.2	E
78	HOMO	-0.1659	1.0000	0	36.3	0	0	57.7	0	0.2	0.2	0.2	0.2	E
79	LUMO	-0.0737	0.0178	0	0	0.4	11.8	0	47.3	11	2.1	1.1	14.2	T_2
80	LUMO+1	-0.0737	0.0178	0	0	57.6	0.7	0	1.3	7.4	3.8	10.8	6.4	T_2
81	LUMO+2	-0.0736	0.0178	0	0	1.5	47	0	10.9	2.9	15.4	9.4	0.8	T_2
82	LUMO+3	0.0126	0.0008	46.4	0	0	0	0	0	11.9	11.9	11.9	11.9	E
#	^{3}[CrF$_4$]	eval	occ	Cr(4s)	Cr(d_{z2})	Cr(d_{xz})	Cr(d_{yz})	Cr(d_{x2y2})	Cr(d_{xy})	F_1	F_2	F_3	F_4	T_d
23*	HOMO-7	-0.3887	2.0000	0	14.8	0	0	3.3	0	20.4	20.5	20.6	20.4	E
24*	HOMO-6	-0.3886	2.0000	0	3.3	0	0	14.8	0	20.4	20.5	20.4	20.5	E
25*	HOMO-5	-0.3886	1.9999	15.8	0	0	0	0	0	21	20.9	20.9	21	A_1
26*	HOMO-4	-0.3653	1.9987	0	0	4.9	5.7	0	16.3	4.6	42.5	13.4	11.9	T_2
27*	HOMO-3	-0.3653	1.9987	0	0	21.3	3.7	0	1.9	12.9	5.8	36.5	18.1	T_2
28*	HOMO-2	-0.3652	1.9987	0	0	0.7	17.5	0	8.7	37.1	6.7	4.6	24.4	T_2
29	HOMO-1	-0.2417	1.0000	0	51.8	0	0	31.4	0	4.2	4.2	4.2	4.2	E
30	HOMO	-0.2417	1.0000	0	31.4	0	0	51.8	0	4.2	4.2	4.1	4.2	E
31	LUMO	-0.1692	0.0014	0	0	2	48.9	0	24.2	11.8	2.9	2.2	8	T_2
32	LUMO+1	-0.1690	0.0013	0	0	59.6	10.3	0	5.4	4.7	2.5	11.7	6.1	T_2
33	LUMO+2	-0.1689	0.0013	0	0	13.6	16	0	45.6	2.2	13.4	4.9	4.4	T_2
34	LUMO+3	-0.0227	0.0001	101.3	0	0	0	0	0	-0.4	-2.1	-0.4	-0.4	A_1
35*	LUMO+4	0.1783	0.0001	0	13	0	0	58.8	0	6.7	6.7	6.7	6.7	E
36*	LUMO+5	0.5546	0.0001	0	58.8	0	0	13	0	6.6	6.7	6.7	6.6	E

*UNOs not shown in Figure 6 (lower right).

Table S13b. BLYP/6-311G* UNOs occupation numbers (occ), including MO eigenvalues (eval), showing the metal and ligand percentage of each orbital and the T_d-like symmetry label for $^3[Cr(NMe_2)_4]$, $^1[Cr(NMe_2)_4]$, and $^3[Cr(OMe)_4]$.

#	$^3[Cr(NMe_2)_4]$	eval	occup	Cr(4s)	Cr(d_{z2})	Cr(d_{xz})	Cr(d_{yz})	Cr(d_{x2-y2})	Cr(d_{xy})	N_1	N_2	N_3	N_4	T_d
55	HOMO-7	-0.2742	1.9999	18.0	0.1	0	0	0.3	0	19.2	23.5	18.8	19.3	A1
56	HOMO-6	-0.2706	1.9998	0	3.3	0	7.5	1.0	0	17.9	21.1	18.0	17.3	T2 / E
57	HOMO-5	-0.2124	1.9997	0.7	3.7	0	0	11.1	0.2	17.2	16.8	17.2	17.0	E
58	HOMO-4	-0.1891	1.9970	0	0	0.4	0	0.4	26.9	18.3	9.8	8.8	18.6	T2
59	HOMO-3	-0.1713	1.9970	0	0	27.2	0.1	0	0.4	9.0	19.0	18.5	8.8	T2
60	HOMO-2	-0.1712	1.9953	0	13.3	0.1	17.5	4.4	0.1	12.2	12.4	12.3	12.2	T2 / E
61	HOMO-1	-0.1285	1.0000	0	32.5	0.1	27.2	22.7	0.3	2.8	2.5	1.8	2.7	T2 / E
62	HOMO	-0.1209	1.0000	1.8	28.7	0	0.6	49.7	0.7	2.5	3.7	3.6	2.5	E
63	LUMO	-0.0561	0.0047	0	16.2	0.1	42.5	5.3	0.1	7.0	7.5	7.0	7.1	T2 / E
64	LUMO+1	-0.0470	0.0030	0	0	66.6	0.2	0	0.7	5.3	8.6	7.3	5.2	T2
65	LUMO+2	-0.0470	0.0030	0	0	0.8	0	1.0	65.9	7.1	6.5	5.3	7.2	T2
66	LUMO+3	0.0101	0.0003	25.1	4.5	0	0	13.5	0.2	7.5	7.7	7.5	7.5	A1 / E
67	LUMO+4	0.0398	0.0002	0	6.3	0	13.2	2.0	0	8.5	9.2	8.4	8.5	T2 / E
68	LUMO+5	0.0399	0.0001	111.6	0.2	0	0	0.6	0	-4.3	-6.2	-4.3	-4.3	A1

#	$^1[Cr(NMe_2)_4]$[a]	eval	occup	Cr(4s)	Cr(d_{z2})	Cr(d_{xz})	Cr(d_{yz})	Cr(d_{x2-y2})	Cr(d_{xy})	N_1	N_2	N_3	N_4	T_d
*21	HOMO-40	-0.7903	2	6.1	0	0	0	0	0	10.5	10.3	10.5	10.3	A1
53	HOMO-8	-0.2765	2	0	0	0	0	0	22.3	10.4	10.3	10.4	10.3	T2
54	HOMO-7	-0.2702	2	7.4	0.2	0	0	0	0	11.8	11.1	11.8	11.1	A1
55	HOMO-6	-0.2678	2	0	0	10.1	10.0	0	0	10.0	10.1	10.0	10.1	T2
56	HOMO-5	-0.2677	2	0	0	10	10.1	0	0	9.8	10.4	9.8	10.4	T2
57	HOMO-4	-0.2105	2	0.1	34.9	0	0	0	0	10.8	10.8	10.8	10.8	E
*58	HOMO-3	-0.1761	2	0	0	0	0	0	2.2	17.3	16.7	17.3	16.7	T2
*59	HOMO-2	-0.1624	2	0	0	3.6	3.7	0	0	17.1	17.0	17.1	17.0	T2
*60	HOMO-1	-0.1624	2	0	0	3.7	3.6	0	0	16.3	17.0	16.3	17.0	T2
61	HOMO	-0.0892	2	0	0	0	0	89.3	0	0.1	0.1	0.1	0.1	E
62	LUMO	-0.0578	0	0.6	61.4	0	0	0	0	6.4	6.4	6.4	6.4	E
63	LUMO+1	-0.0331	0	0	0	28.2	28.7	0	0	5.7	5.8	5.7	5.8	T2
64	LUMO+2	-0.0330	0	0	0	28.6	28.2	0	0	5.8	5.7	5.8	5.7	T2
65	LUMO+3	-0.0065	0	0	0	0	0	0	50.9	3.0	3.0	3.0	3.0	T2
66	LUMO+4	0.0102	0	10.9	1.1	0	0	0	0	1.2	1.2	1.2	1.2	A1
67	LUMO+5	0.0447	0	0	0	0	0	0	15.4	1.4	1.4	1.4	1.4	T2
68	LUMO+6	0.0453	0	0	0	1.5	1.7	0	0	0.9	1.0	0.9	1.0	T2
69	LUMO+7	0.0453	0	0	0	1.7	1.5	0	0	1.0	1.0	1.0	1.0	T2

#	$^3[Cr(OMe)_4]$	eval	occup	Cr(4s)	Cr(d_{z2})	Cr(d_{xz})	Cr(d_{yz})	Cr(d_{x2-y2})	Cr(d_{xy})	O_1	O_2	O_3	O_4	T_d
39	HOMO-7	-0.2671	1.9999	12	0.1	0.1	0.1	1.6	0	11.7	27.2	16.5	22.7	A1
40	HOMO-6	-0.2531	1.9999	2.2	0.7	1.3	0.7	10.5	0	27.1	10.3	20.7	15.1	E
41	HOMO-5	-0.2455	1.9999	0	12.3	2.3	0.1	2.4	0.2	5.9	13.0	9.9	42.4	E
42	HOMO-4	-0.2370	1.9980	0.1	3.0	13.2	0.3	1.9	11.6	3.9	11.1	9.0	31.8	T2
43	HOMO-3	-0.2293	1.9976	0	2.4	4.7	9.6	0.8	13	13.5	10.6	27.6	4.5	T2
44	HOMO-2	-0.2229	1.9973	0.1	2.4	4.5	17.5	1.2	3.4	30.2	19.9	5.8	1.4	T2
45	HOMO-1	-0.1540	1.0000	0.1	5.5	4.3	3.3	69.7	0.1	3.9	2.8	2.8	2.6	E
46	HOMO	-0.1439	1.0000	0	63.9	8.9	0.5	7.4	0.4	1.7	3.1	2.8	6.6	E
47	LUMO	-0.0801	0.0027	0	2.8	12.7	43.9	1.3	9.0	12.6	8.0	3.1	1.4	T2
48	LUMO+1	-0.0722	0.0024	0	2.7	11.9	21.2	1.4	32.1	5.9	5.7	11.6	2.4	T2
49	LUMO+2	-0.0691	0.0020	0	4.5	34.1	1.1	1.5	28.4	1.9	5.6	3.8	13.3	T2
50	LUMO+3	0.0067	0.0001	0	24.4	5.0	0.5	4.1	0.1	4.6	1.2	1.8	9.4	E
51	LUMO+4	0.0394	0.0001	9.2	2.0	2.0	2.8	23.2	0.1	3.1	5.0	4.8	5.0	E
52	LUMO+5	0.0438	0.0001	47.8	0.1	0	0	4.5	0.1	6.8	9.5	6.5	8.6	A1

*UNOs not shown in Figure S10.

[a] In the case of $^1[Cr(NMe_2)_4]$ MOs are presented.

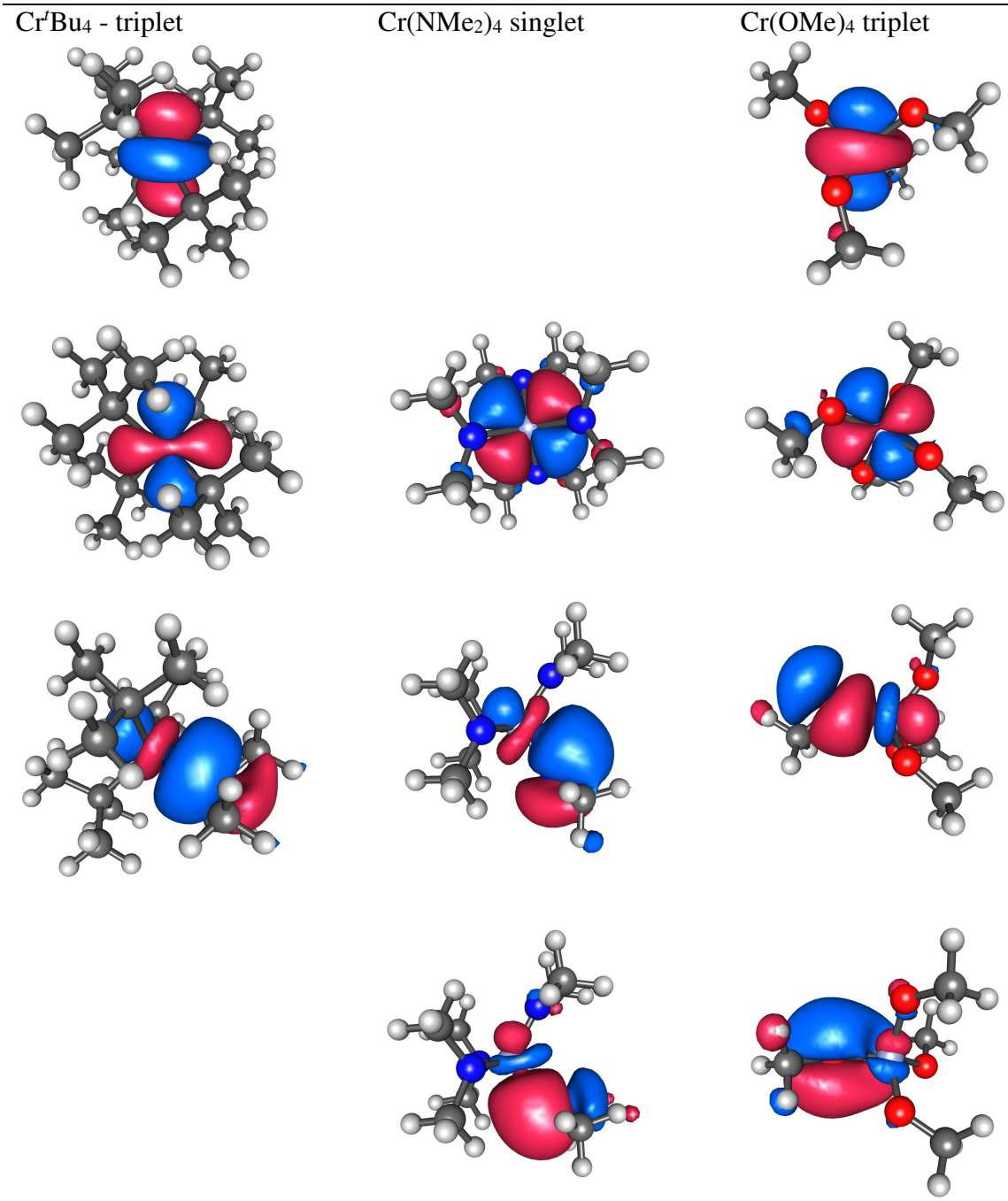

Figure S8. Localized BLYP/6-311G* orbitals for ^{3}[Cr^{t}Bu$_4$] (left column), ^{1}[Cr(NMe$_2$)$_4$] (middle column), ^{3}[Cr(OMe)$_4$] (right column). Population of the Cr-X bonding orbitals on the central Cr atom are given in Table S7. Color scheme: H - white, C - grey, N - blue, O - red, Cr - light blue.

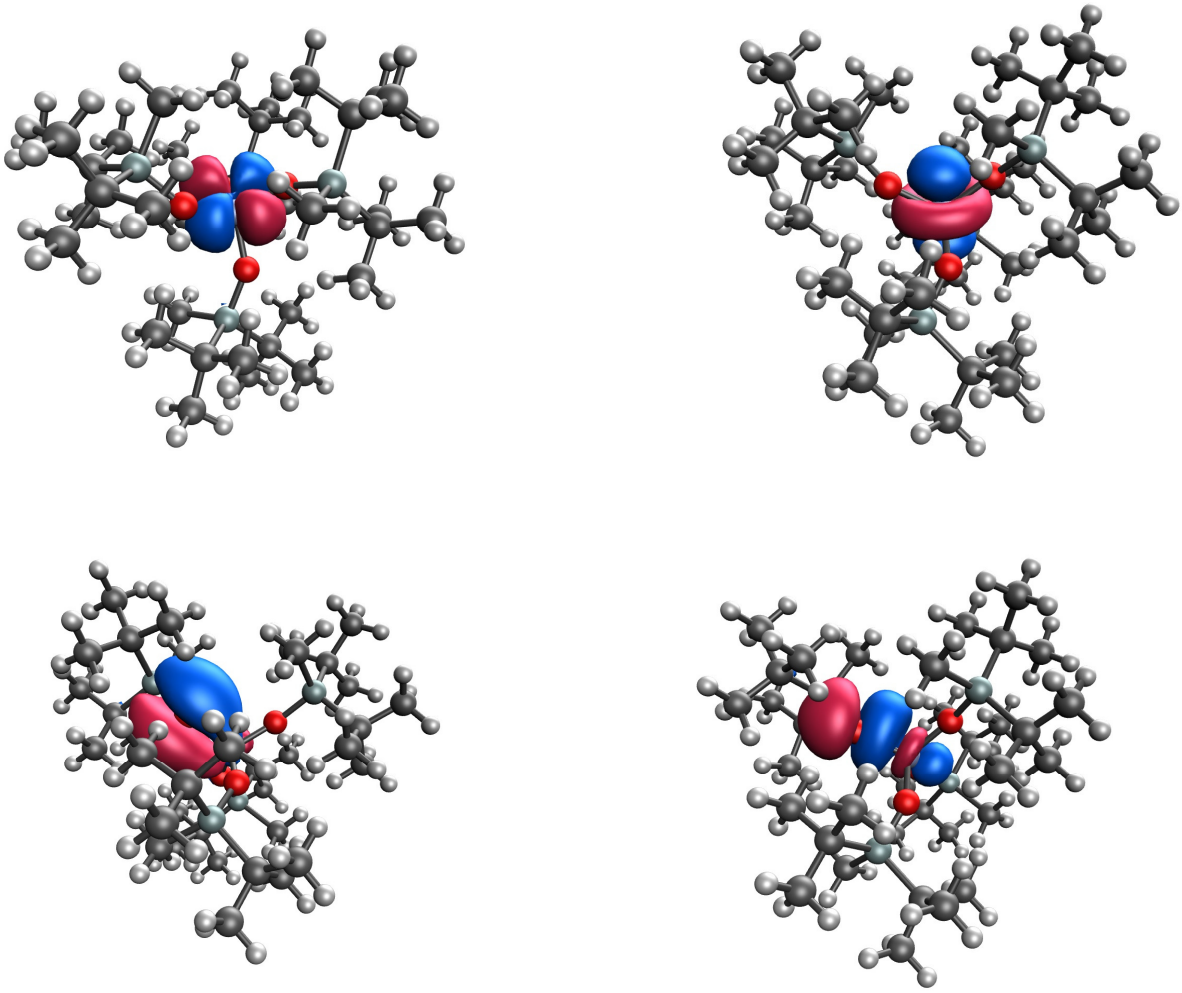

Figure S9. Localized BLYP/6-311G* orbitals of $Cr(DTBMS)_4$. Population of the Cr-X bonding orbitals on the central Cr atom are given in Table S7. Color scheme: H - white, C - grey, O - red, Si - light grey, Cr - light blue.

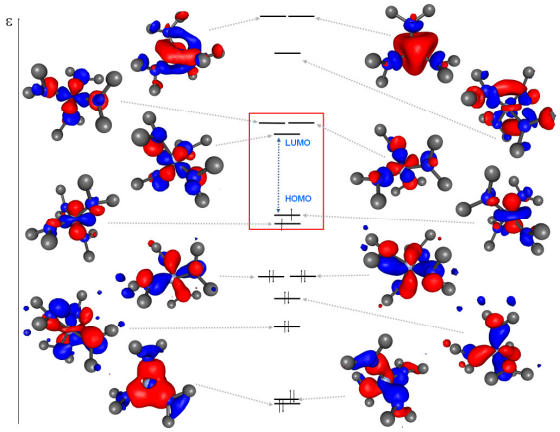

$^3[Cr(NMe_2)_4$ - Triplet

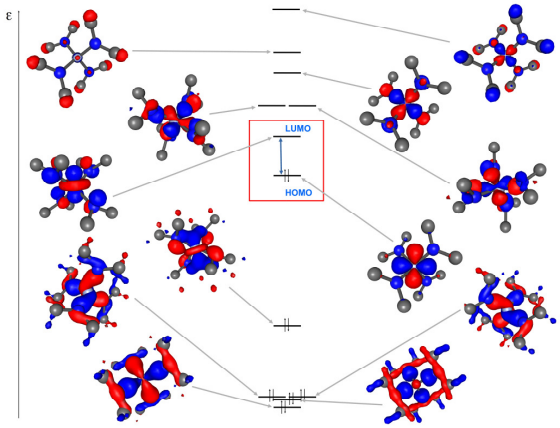

$^1[Cr(NMe_2)_4]$ - Singlet

Figure S10. BLYP/6-311G* UNOs of $^3[Cr(NMe_2)_4]$ (triplet ground state, top) and FMOs of $^1[Cr(NMe_2)_4]$ (singlet ground state, bottom). It can be seen that HOMO eigenvalue in $Cr(NMe_2)_4$ raise for the singlet comparing to triplet state, while the lower occupied frontier orbitals become stabilized in the case of singlet states.

V. Spin Hamiltonian parameters: Excited state SOC contributions to zfs

As discussed in the main text, there are only a few excited states that contribute significantly to zfs via SOC, while spin-spin coupling (SSC) contributions are negligible (compare CASSCF and $MRCI_{MIN}$ results in Table S14 or Table 4 main text). This is evident in Table S15, where we focus on the sole complex for which the zfs has been definitively determined, and is the largest, namely $Cr(DTBMS)_4$. Roots 1, 2, and 3 of block 0 in Table S15a correspond to the $^3T_2$ excited state (in T_d), which spits into three roots, two of which correspond to ^3E (in D_{2d}) and one to $^3B_2$. The former contribute positively to D^{SOC}, while the latter contributes negatively, as given by Eqn 4. As expected from the relatively modest distortion of $Cr(DTBMS)_4$ from ideal tetrahedral geometry, the magnitude of these two counteracting contributions is relatively close (+6.7 versus −5.9 cm^{-1}, respectively). The actual geometry is not D_{2d}, so the ^3E state orbital degeneracy is removed with its components contributing oppositely to give E^{SOC} (roots 1 and 2 of block 0 in Table S13b nearly cancel out). Roots 2, 3, and 5 of block 1 (Table S15a) correspond to the $^1T_2(D)$ excited state, which behaves exactly as in Eqn 4, wherein the contributions to D^{SOC} from ^1E are negative, while those from $^1B_2$ are positive (respectively −2.6 and +2.4 cm^{-1}). Roots 2 and 3 of block 1 in Table S13b are the nearly cancelling contributions to E^{SOC} from the lower symmetry splitting of $^1E(^1T_1(D))$. Last and least come roots 11, 12, and 13 of block 1, which correspond to the contributions to D^{SOC} from the $^1T_2(G)$ excited state, behaving exactly as $^1T_2(D)$ does, except with smaller magnitudes as it is much higher in energy (see Figures 5 and S1). Roots 12 and 13 of block 1 in Table S15b are the corresponding contributions to E^{SOC}. The sum of contributions to D^{SOC} from these three T_2 excited states equals +0.682 cm^{-1}, while that from the remaining excited states is a negligible +0.01 cm^{-1}, a value that is less than the precision of the HFEPR experiment. The situation for E^{SOC} is similar: +0.069 cm^{-1} from these three out of a total of 0.070 cm^{-1}. Thus, the classical perturbation theory

expression in Eqn 4 is more than sufficient for calculating zfs in such systems – provided the excited state energies are known, which is far from routine. The paradox, so to speak, is that the zfs depends on the relative energies of the $^{1,3}T_2$ excited states, but the energy of $^3T_1(F)$ excited state is the only one readily obtained from electronic absorption spectra of CrL_4 complexes. The ability in $Cr(DTBMS)_4$ to assign bands due to $^3T_2$ and $^1T_1(G)$ is crucial in being able to analyze the electronic structure of this complex successfully.

Table S14. Calculated spin Hamiltonian (zfs and **g**-tensor) parameters in the 6-311G* basis set. (In parentheses are shown the results of the CASSCF state averaged calculations, taking the singlet state as a reference for the amidos under investigation). Relevant experimental data are also given.

		D (cm^{-1})	E (cm^{-1})	g_{xx}	g_{yy}	g_{zz}	g_{iso}
CrF_4	BLYP	–0.011	–0.003	1.977	1.977	1.977	1.977
	CASSCF	–0.016	–0.004	1.926	1.926	1.926	1.926
	$MRCI_{MIN}$	–0.019	–0.005				
	NEVPT2	–0.022	–0.001	1.936	1.936	1.937	1.936
Alkyl Complexes							
$Cr(Nor)_4$ [a]	expt. I	0.027	0.0041				(1.9905)
	expt. II	0.023	0.0027				
	expt. III	0.013	0.0032				
	expt. IV	0.012	0.0029				
$Cr(CH_2SiMe_3)_4$	BLYP	–0.058	–0.014	1.991	1.992	1.992	1.992
	CASSCF	+0.092	+0.026	1.950	1.951	1.952	1.951
	$MRCI_{MIN}$	+0.097	+0.081				
Cr^tBu_4	BLYP	+0.001	0.000	1.993	1.993	1.993	1.993
	CASSCF	+0.005	+0.001	1.947	1.948	1.948	1.948
	MRCI	+0.005	+0.001				
Amido Complexes							
$Cr(NMeCH^tBu_2)_4$	BLYP	+1.459	+0.143	1.975	1.982	1.987	1.981
	CASSCF	–62.730	–0.663	1.191	1.862	1.882	1.645
		(–7.733)	(–1.141)	(1.835)	(1.916)	(1.953)	(1.901)
	$MRCI_{MIN}$	–63.321	–0.777				
	NEVPT2	–9.776	–0.420	1.802	1.953	1.963	1.906
$Cr(NMe_2)_4$	BLYP	-0.042	0.000	1.985	1.987	1.987	1.987
	CASSCF	-0.935	0.002	1.938	1.954	1.954	1.949
	MRCI	-0.992	0.002				
$Cr(NMe_2)_4$	BLYP	–1.827	–0.204	1.971	1.985	1.994	1.983
C_2 symm.	CASSCF	–154.369	–0.882	0.625	1.604	1.619	1.283
		(+2.407)	(+0.005)	(1.928)	(1.929)	(1.962)	(1.940)
	MRCI	–155.346	-0.877				
	NEVPT2	–1.953	-0.356	1.820	1.953	1.973	1.915
Alkoxido Complexes							
$Cr(OCH^tBu_2)_4$ [b]	BLYP	–0.564	0.000	1.968	1.978	1.978	1.975
		–0.589 [b]	0.000 [b]				
	CASSCF	–2.045	–0.001	1.896	1.927	1.927	1.917
		–2.193 [b]	0.000 [b]				
	$MRCI_{MIN}$	–2.087	–0.001				
		–2.238 [b]	0.000 [b]				

$Cr(O^tBu)_4$ [b]	BLYP	+0.868	0.000	1.974	1.974	1.984	1.977
		+0.915 [b]	0.000 [b]				
	CASSCF	+1.772	0.000	1.920	1.920	1.947	1.929
		+1.828 [b]	0.000 [b]				
	$MRCI_{MIN}$	+1.780	0.000				
		+1.867 [b]	0.000 [b]				
	expt.[c]	(< 0.3)					1.962
$Cr(OMe)_4$	BLYP	+1.249	+0.172	1.980	1.982	1.985	1.982
	CASSCF	+1.173	+0.084	1.931	1.935	1.952	1.939
	$MRCI_{MIN}$	+1.492	+0.084				
	NEVPT2	+0.905	+0.046	1.943	1.948	1.961	1.951
Siloxido Complexes							
$Cr(OSiMe_3)_4$	BLYP	0.352	0.000	1.972	1.972	1.976	1.974
	CASSCF	+0.789	0.000	1.920	1.920	1.931	1.923
	$MRCI_{MIN}$	+0.804	0.000				
	NEVPT2	+0.748	0.000	1.929	1.929	1.941	1.933
$Cr(DTBMS)_4$	BLYP	+0.287	+0.028	1.972	1.972	1.975	1.973
Experimental geometry	CASSCF	+0.704	+0.072	1.915	1.918	1.927	1.920
	$MRCI_{MIN}$	+0.719	+0.080				
$Cr(DTBMS)_4$	BLYP	+0.098	+0.002	1.9702	1.9702	1.9721	1.9708
Optimized geometry	CASSCF	+0.425	+0.006	1.9127	1.9128	1.9185	1.9146
	$MRCI_{MIN}$	+0.432	+0.006				
	expt.[d]	+0.556	0.0	1.935	1.935	1.9	1.92

[a] Taken from Ward et al.[1] Four conformations were identified (denoted I – IV) for $Cr(Nor)_4$ in frozen isooctane solution at 93 K and the zfs parameters for each is given (no sign determination was possible, hence no sign is provided). The *g* value given is from a single crystal measurement at room temperature and thus does not directly correspond to the frozen solution data.

[b] The second set of zfs parameters given for each theory model corresponds to use of the optimized structure for each of $Cr(OCH^tBu_2)_4$ and $Cr(O^tBu)_4$, but then with the substituents converted to simply methyl groups, allowing direct comparison with "authentic" $Cr(OMe)_4$.

[c] Taken from Alyea et al.[7] There was evidence for small magnitude zfs, but its value was not determined. Its magnitude must be smaller than the X-band microwave quantum energy, hence the upper limit provided.

[d] The experimental value for only species B (the major one) is given here; see Table 1 for the full dataset.

Table S15. CASSCF/6-311G* and NEVPT2/6-311G* zfs contributions for selected CrL_4 complexes: **a)** *D* and, **b)** *E* parameters; all values in cm^{-1}.

a) *D*			CASSCF					NEVPT2		
Block	Mult	Root	CrF_4 [a]	Cr^tBu_4	$Cr(NMe_2)_4$	$Cr(OMe)_4$	$Cr(DTBMS)_4$	CrF_4 [a]	$Cr(NMe_2)_4$	$Cr(OMe)_4$
0	3	0	0	0	0	0	0	0	-14.148	0
0	3	1	-2.357	1.935	-158.773	1.92	3.382	-4.586	0	1.438
0	3	2	2.812	1.941	1.711	2.306	3.315	2.46	0.707	1.876
0	3	3	-0.475	-3.869	0.001	-2.815	-5.885	2.098	0.621	-2.138
0	3	4	0	0	-0.295	0.037	0.001	0	0	0.033
0	3	5	0	0	0.24	0.008	0	0	0.828	0.007
0	3	6	0	0	1.66	-0.002	0.001	0	0.005	-0.002
0	3	7	0	0	0	-0.001	0	0	0.185	-0.001
0	3	8	0	0	0.057	0	0	0	0.016	0
0	3	9	0	0	-0.004	0	0	0	0	0
1	1	0	0	0	0	0.002	0.001	0	8.81	0.004
1	1	1	0	0	3.46	0.001	0	0	0.002	0.001
1	1	2	-0.001	-0.973	0.002	-0.34	-1.309	-0.002	2.13	-0.27
1	1	3	2.15	-0.933	-0.007	-0.379	-1.296	2.432	-0.151	-0.418
1	1	4	-1.061	1.904	0	-1.096	0.011	-1.24	0.347	-1.062
1	1	5	-1.084	0	0.398	1.555	2.425	-1.183	0	1.47
1	1	6	0	0	-0.782	-0.019	-0.003	0	-0.487	-0.018
1	1	7	0	0	0	0.007	-0.002	0	0.01	0.008
1	1	8	0	0	-0.831	-0.016	0	0	-0.145	-0.017
1	1	9	0	0	-0.086	-0.002	0	0	-0.437	-0.002
1	1	10	0	0	-0.136	0.013	0.001	0	-0.246	0.011
1	1	11	-0.018	0.02	-0.154	0.033	0.151	-0.05	-0.043	0.031
1	1	12	-0.049	-0.01	0	-0.036	-0.051	-0.05	0.001	-0.035
1	1	13	0.067	-0.011	0.015	-0.028	-0.050	0.099	0	-0.026
1	1	14	0	0	0	0.001	0	0	0.025	0.001
Totals			−0.016	+0.004	−153.5	+1.149	+0.692	-0.022	−1.970	+0.891

b) *E*			CASSCF					NEVPT2		
Block	Mult	Root	CrF_4 [a]	Cr^tBu_4	$Cr(NMe_2)_4$	$Cr(OMe)_4$	$Cr(DTBMS)_4$	CrF_4 [a]	$Cr(NMe_2)_4$	$Cr(OMe)_4$
0	3	0	0	0	0	0	0	0	0	0
0	3	1	0.667	1.936	0	1.708	2.761	0.088	0	-0.251
0	3	2	-0.761	-1.937	-1.711	-1.468	-2.679	0.728	-0.707	0.572
0	3	3	0.088	0.002	0.001	-0.152	0	-0.819	0.621	-0.34
0	3	4	0	0	0	0.033	0.001	0	0	0.031
0	3	5	0	0	-0.24	-0.012	0	0	-0.828	-0.001
0	3	6	0	0	1.66	-0.001	-0.001	0	0.005	0
0	3	7	0	0	0	0	0	0	0.185	0
0	3	8	0	0	-0.057	0	0	0	-0.016	0
0	3	9	0	0	0	0	0	0	0	0
1	1	0	0	0	0	-0.002	0	0	0	0.004
1	1	1	0	0	0	0	0	0	0	0
1	1	2	0.001	-0.86	0	-0.565	-1.222	0.001	0	0
1	1	3	-0.002	0.846	-0.007	-0.34	1.208	-0.013	-0.151	0.013
1	1	4	1.17	0.014	0	0.887	0	1.176	0	0.021
1	1	5	-1.168	0	0	-0.027	0	-1.163	0	0.015
1	1	6	0	0	0.782	0.006	0.001	0	0.487	0.02
1	1	7	0	0	0	0.025	0	0	0	-0.012
1	1	8	0	0	-0.831	-0.013	0	0	-0.145	-0.028
1	1	9	0	0	0.086	-0.002	0	0	0.437	0
1	1	10	0	0	-0.136	-0.003	0	0	-0.246	-0.002
1	1	11	-0.029	0	0.154	0	0	-0.015	0.043	-0.001
1	1	12	0.033	0.01	0	0.035	0.050	0.016	0	0.029
1	1	13	-0.004	-0.01	0	-0.023	-0.049	0	0	-0.025
1	1	14	0	0	0	0	0	0	0	0
Totals			−0.005	+0.001	−0.299	+0.086	+0.070	−0.001	−0.315	+0.045

[a] 6-311+G* basis set

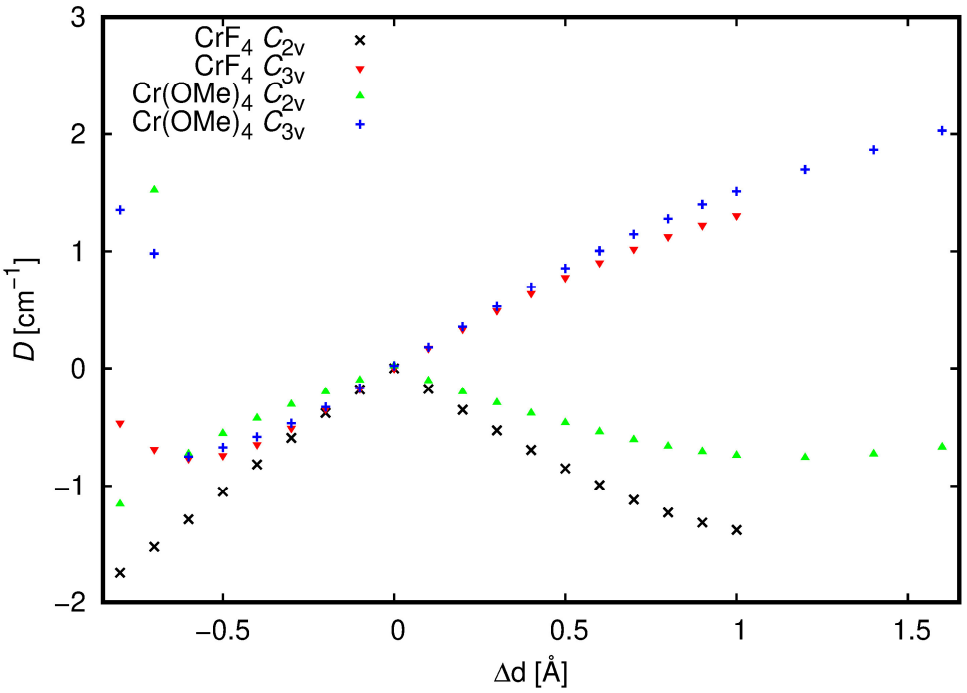

Figure S11. BLYP/6-311G* D parameter dependence upon geometrical distortion of bond lengths for $Cr(OMe)_4$ and CrF_4 taking the T_d geometry as reference. Positive change means bond shortening.

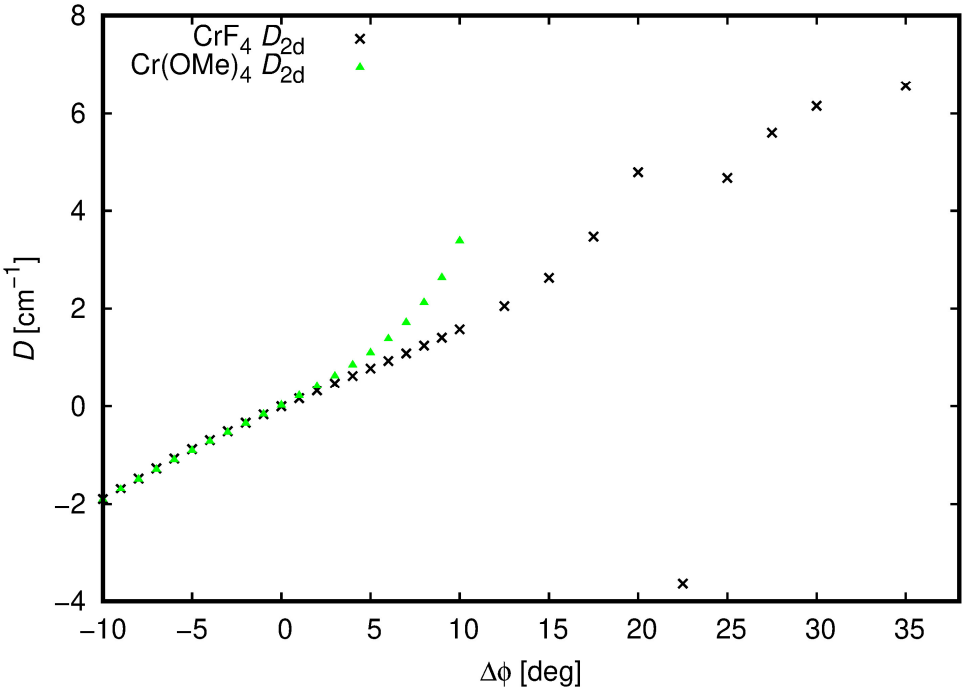

Figure S12. BLYP/6-311G* D parameter dependence upon geometrical distortion of bond angles for $Cr(OMe)_4$ and CrF_4. Positive change means angle opening.

VI. Discussion of electronic absorption spectra of CrL_4 complexes.

Cr^tBu_4 exhibits calculated bands at ~12 660 and 19 800 cm^{-1}, the latter of which is quite close to those reported for several CrR_4 complexes,[3] as described above. The former calculated band (at 790 nm) might not be observable. For the alkoxides, the results are reasonable in that for $Cr(OMe)_4$, the main visible band is calculated at ~13 700 or ~17 000 cm^{-1}, respectively using CASSCF and NEVPT2 levels of theory, versus 15 200 cm^{-1} experimentally for $Cr(O^tBu)_4$.[7] A calculated spectrum for $Cr(O^tBu)_4$ is shown in Figure S24. A NIR band is also calculated (11 580 cm^{-1} by CASSCF), although substantially blue shifted from experiment (9100 cm^{-1}). The amido complex $Cr(NMe_2)_4$ in the triplet ground state exhibits a calculated band at ~650 nm (Figure S16) that is in the range of that observed experimentally (730 nm, 13 700 cm^{-1}), regardless of R group.[11] The band calculated for $Cr(NMeCH^tBu_2)_4$ is more red-shifted (Figure S22), in closer agreement to experiment. However, calculated bands in the region of 18 000 cm^{-1} are not observed, which is essentially the problem originally pointed out by Basi et al.[11] The electronic absorption spectra of tetraamido complexes of Cr^{IV} thus remain mysterious. Lastly, the siloxide complex $Cr(DTBMS)_4$, which could be calculated only using CASSCF, gave reasonable correspondence with experiment. In addition to the CT bands above 28 000 cm^{-1}, there are calculated bands at ~17 000, ~11 600, and ~10 000 cm^{-1} (Table S12; see also Figure S28), which correspond roughly to the observed bands at 18 520, 12 500, and 9600 – 8700 cm^{-1}.[14] As seen in the alkoxide $Cr(O^tBu)_4$, CASSCF-calculated bands are generally red shifted from experiment, so this correspondence is acceptable.

VII. Discussion of vibrational spectra of CrL_4 complexes.

Vibrational, as well as electronic, transitions of the systems under study are presented in Figures S13 – S28. As their analysis is a complicated task, we will restrict our discussion to the vibrations of the central CrX_4 (X = F, O, N, or C) part of simple triplet state complexes, namely $Cr(ER_n)_4$, E = F, OR, NR_2, CR_3, R = Me, n = 0 – 3, as in larger molecules (i.e., more complex R groups) the central part vibrations (ν(Cr-X)) of interest become hardly distinguishable from the primarily ligand ones (ν(C-O, C-N, C-C), etc.).

The optimized geometry of $^3[CrF_4]^0$ is nearly of T_d symmetry. The lowest two scissoring vibrations (calculated at 189 and 191 cm^{-1}) of low intensity originate in IR forbidden E(T_d) vibrations (ν_2). The next three higher wagging vibrations (199, 202, and 202 cm^{-1}) of medium intensity, and the highest three asymmetric stretching vibrations (772, 773, and 776 cm^{-1}) of high intensity correspond to the IR allowed $T_2(T_d)$ ones, respectively ν_4 and ν_3. The unobserved symmetric stretching vibration at 703 cm^{-1} corresponds to the IR forbidden $A_1(T_d)$ one (ν_1). These results are in good agreement with Schlöder et al., who calculated ν_3 at 783.5 cm^{-1} and ν_1 at 713.9 cm^{-1} (using B3LYP basis set; respectively at 799.7 cm^{-1} and 722.1 cm^{-1} using CCSD(T)),[42] and with their experiment, which gave ν_3 at 784.3 cm^{-1} in an Ar matrix (790.2 cm^{-1} in a Ne matrix). It can be expected that only the analogs of both these $T_2(T_d)$ vibration types corresponding to the central CrE_4 part of the studied complexes might be observed in calculated IR spectra.

Concerning the alkyl complex, $^3[Cr^tBu_4]^{0.}$ we found only three medium intense vibrations (at 1161, 1162, and 1163 cm^{-1}) of the CrC_4 core. The IR forbidden Cr-C symmetric stretching vibrations were at 227 and 1187 cm^{-1}. In $^3[Cr(CH_2SiMe_3)_4]^{0.}$ we identified two weak (at 542 and 544 cm^{-1}), a single weak, higher (at 563 cm^{-1}), three medium intense (at 711, 711, and 712 cm^{-1}), and

four medium intense, higher (at 982, 985, 990. and 992 cm^{-1}) vibrations. For the amido complex, $^3[Cr(NMe_2)_4]^{0.}$ we found three intense (at 587, 595, and 608 cm^{-1}), three very intense (at 960. 963, and 963 cm^{-1}), three less intense (at 1175, 1176, and 1186 cm^{-1}), and again three less intense (1279, 1279, and 1282 cm^{-1}) CrN_4 vibrations. The IR forbidden Cr-N symmetric stretch was calculated at 978 cm^{-1}.

In the alkoxide complex, $^3[Cr(OMe)_4]^0$, we identified three medium intense vibrations (at 653, 685, and 687 cm^{-1}), two very intense (1065 and 1970 cm^{-1}) and again two medium intense (1977 and 1096 cm^{-1}) vibrations of the CrO_4 core. The IR forbidden Cr-O symmetric stretch was at 601 cm^{-1}. Nevertheless, in the larger complex, $^3[Cr(O^tBu)_4]^0$, we may see three medium intense (at 625, 634, and 634 cm^{-1}) and three very intense (942, 944, and 944 cm^{-1}) core vibrations in agreement with the above CrF_4 scheme. The IR forbidden Cr-O symmetric stretch was again at 601 cm^{-1}. The red shifted, very intense vibrations in $^3[Cr(O^tBu)_4]^0$ relative to $^3[Cr(OMe)_4]^0$ might be explained by Cr-O bond weakening due to the bulky $^-O^tBu$ ligands.

In the smaller siloxide complex, $^3[Cr(OSiMe_3)_4]^0$, we were able to identify only three very intense vibrations (at 911, 915, and 915 cm^{-1}). The IR forbidden Cr-O symmetric stretch was calculated at 1036 cm^{-1}. In the larger one, $^3[Cr(OSiMe^tBu_2)_4]^0$ ($Cr(DTBMS)_4$), we found only three very intense vibrations at 868 cm^{-1}. The red shifted very intense vibrations in the larger siloxide complex relative to the smaller one might be again explained by Cr-O bond weakening due to the bulkier ligand.

Finally, it may be concluded that some CrX_4 skeleton features derived from CrF_4 might be observed in all complexes under study. Mixing of CrX_4 and ligand vibrations (especially for bulky ligands) makes their resolution problematic and is the source of the qualitative differences among the studied molecules.

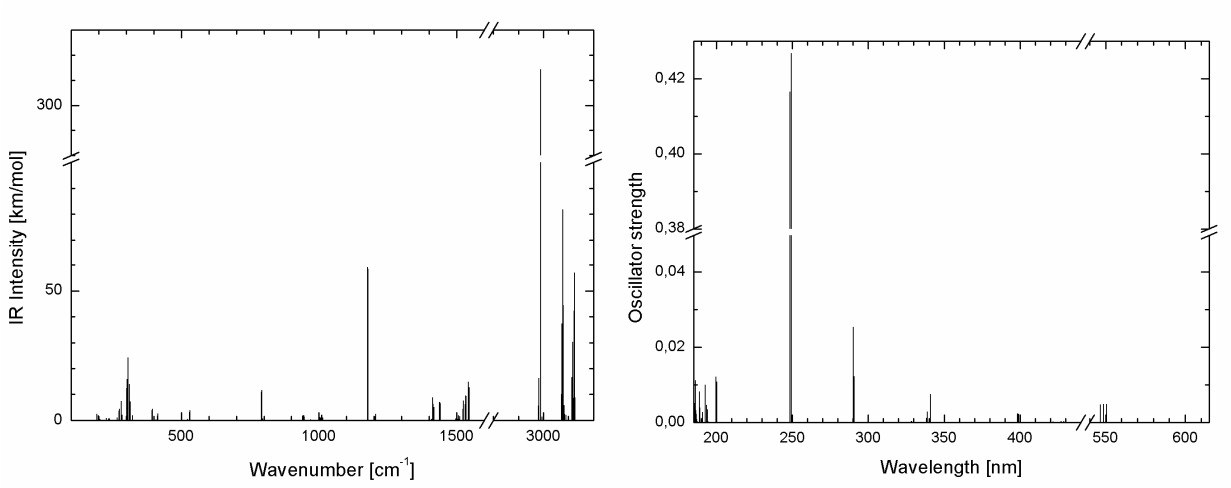

Figure S13. $^{1}[Cr^{t}Bu_4]^0 = {}^{1}[Cr(CMe_3)_4]^0$ (UB3LYP/6-311G*)

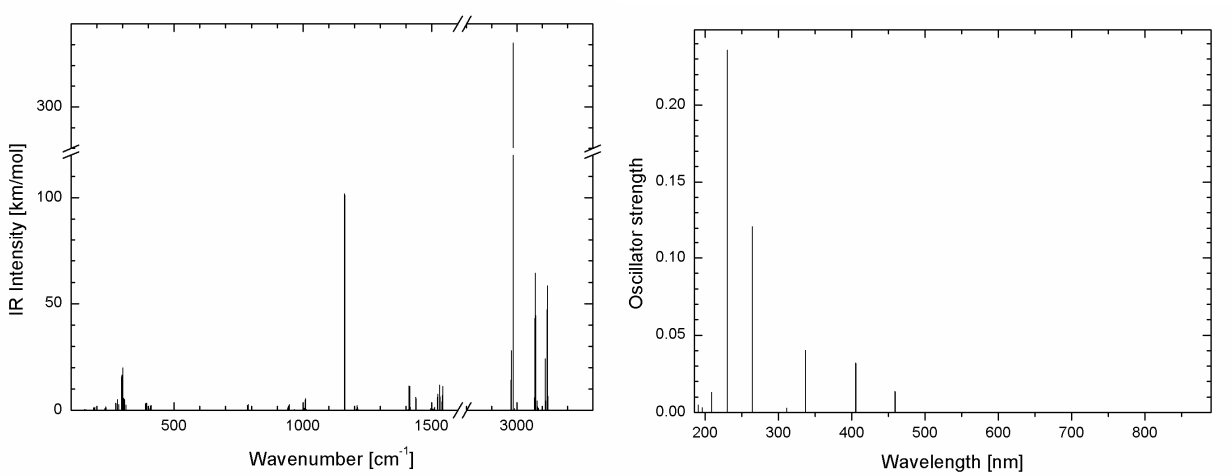

Figure S14. $^{3}[Cr^{t}Bu_4]^0 = {}^{3}[Cr(CMe_3)_4]^0$

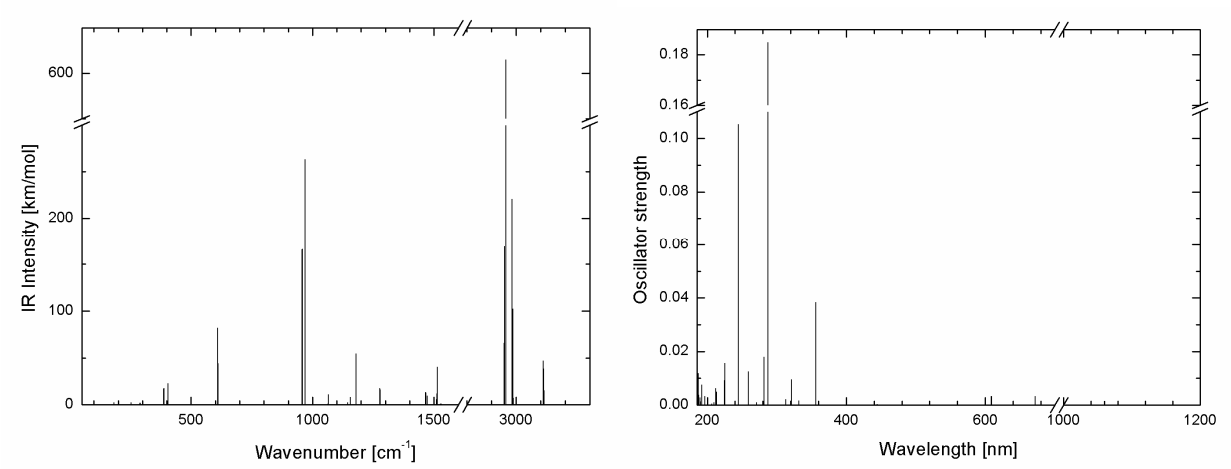

Figure S15. $^{1}[Cr(NMet_2)_4]^0$ (UB3LYP/6-311G*)

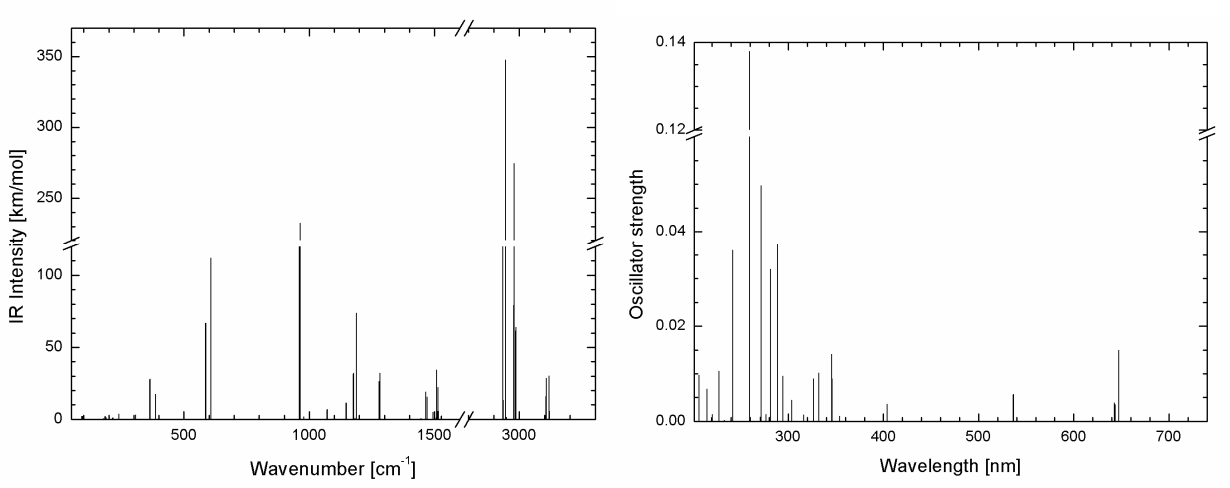

Figure S16. $^3[Cr(NMe_2)_4]^0$

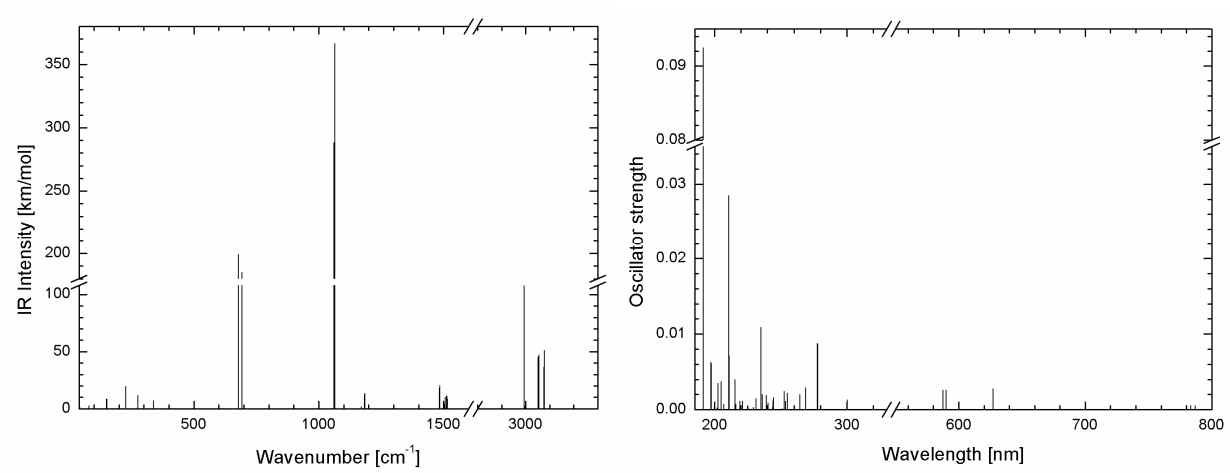

Figure S17. $^1[Cr(OMe)_4]^0 = {}^1[Cr(OCH_3)_4]^0$ (UB3LYP/6-311G*)

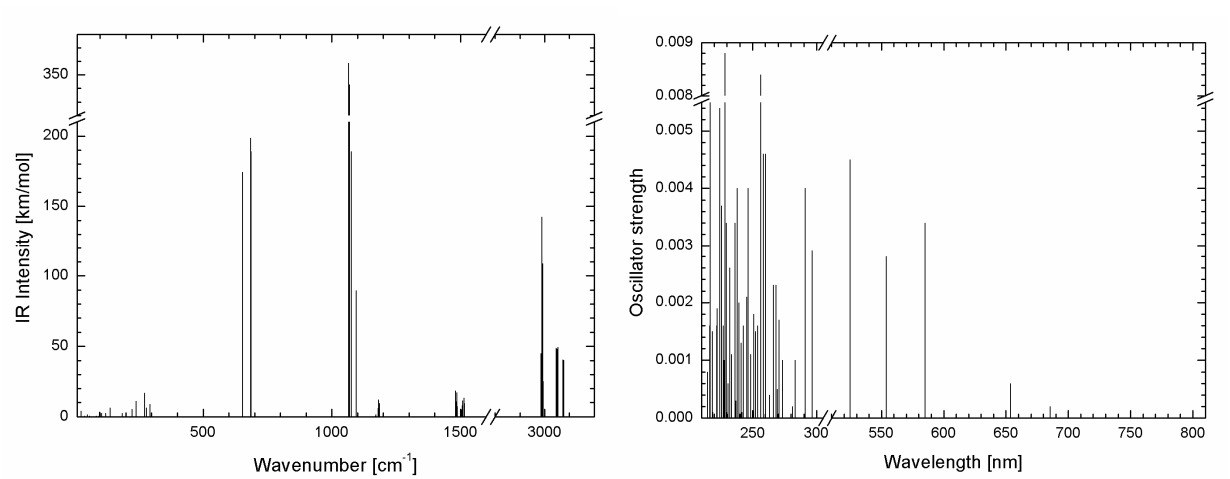

Figure S18. $^3[Cr(OMe_4)]^0 = {}^3[Cr(OCH_3)_4]^0$

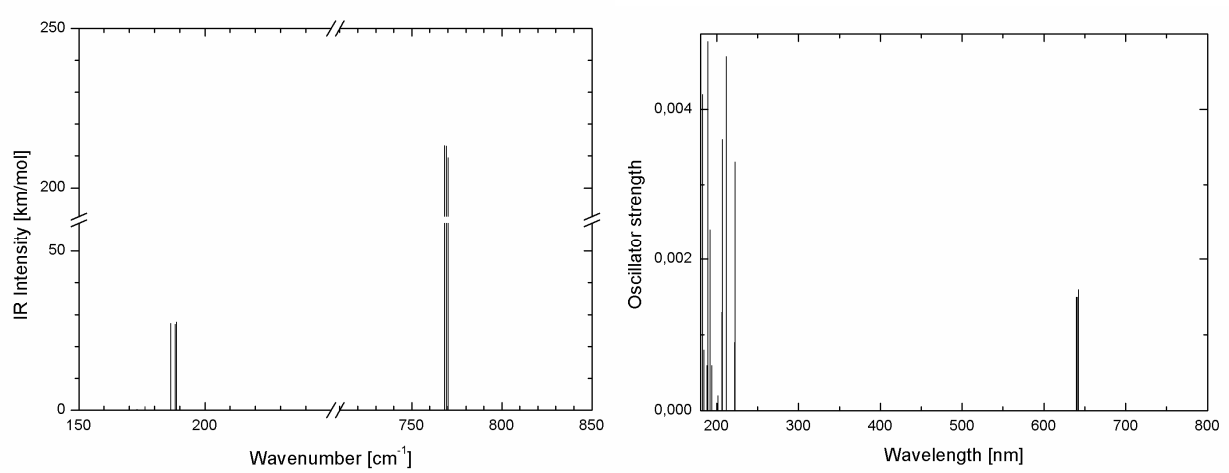

Figure S19. $^1[CrF_4]^0$ (UB3LYP/6-311+G*)

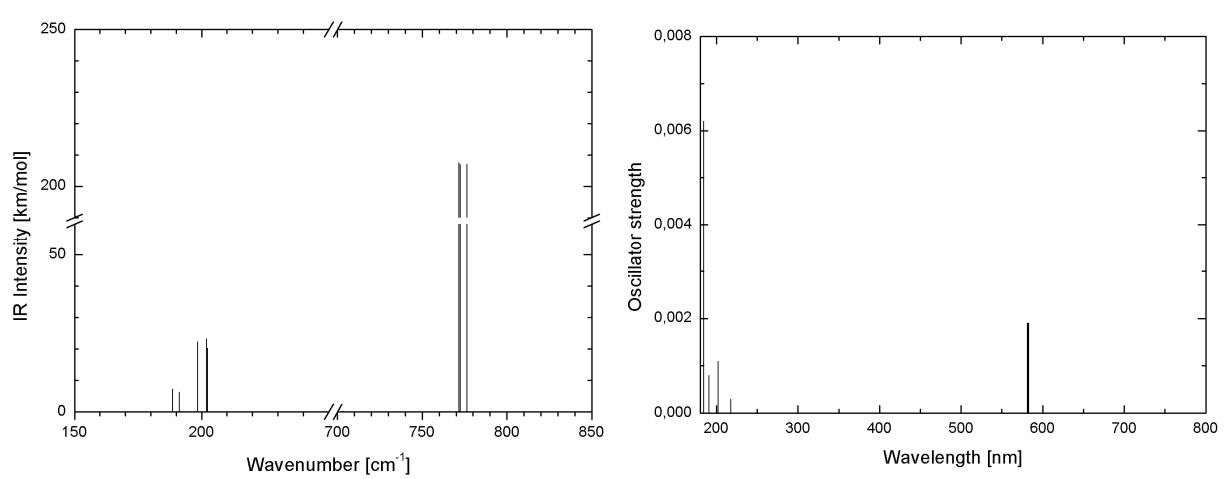

Figure S20. $^3[CrF_4]^0$

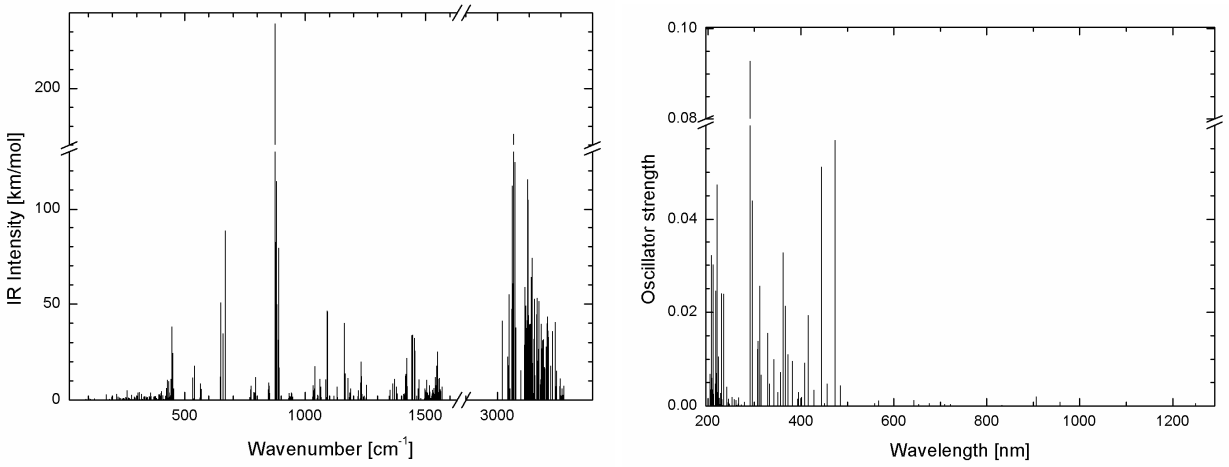

Figure S21. $^1[Cr(NMeCH^tBu_2)_4]^0$ (UB3LYP/6-311G*)

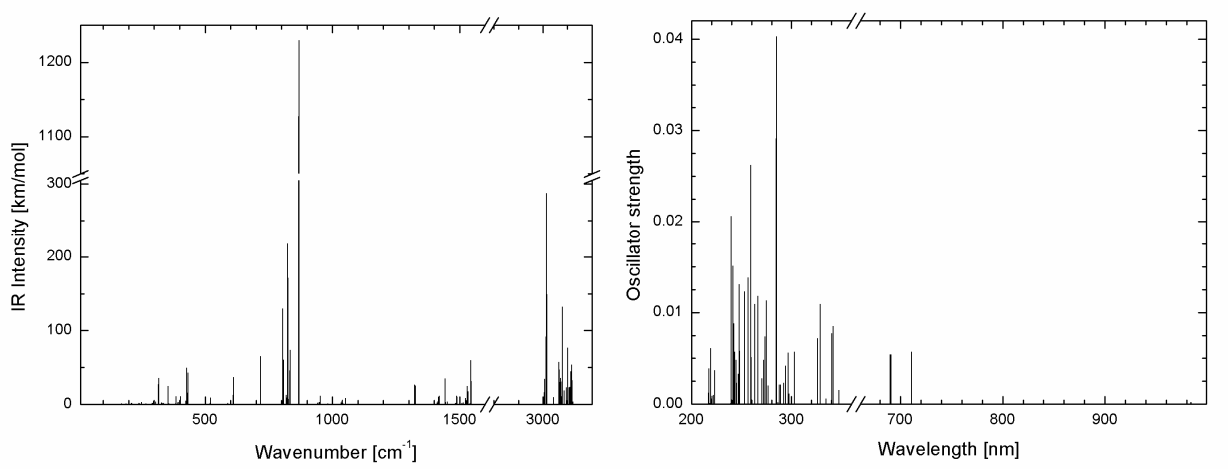

Figure S22. $^3[Cr(NMeCH^tBu_2)_4]^0$

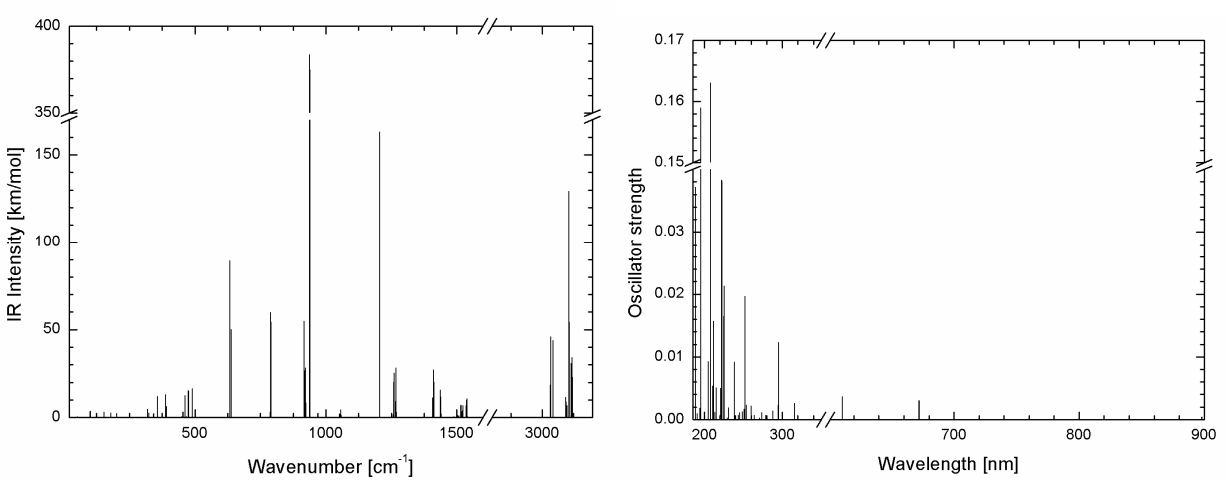

Figure S23. $^1[Cr(O^tBu)_4]^0 = {}^1[Cr(OCMe_3)_4]^0$ (UB3LYP/6-311G*)

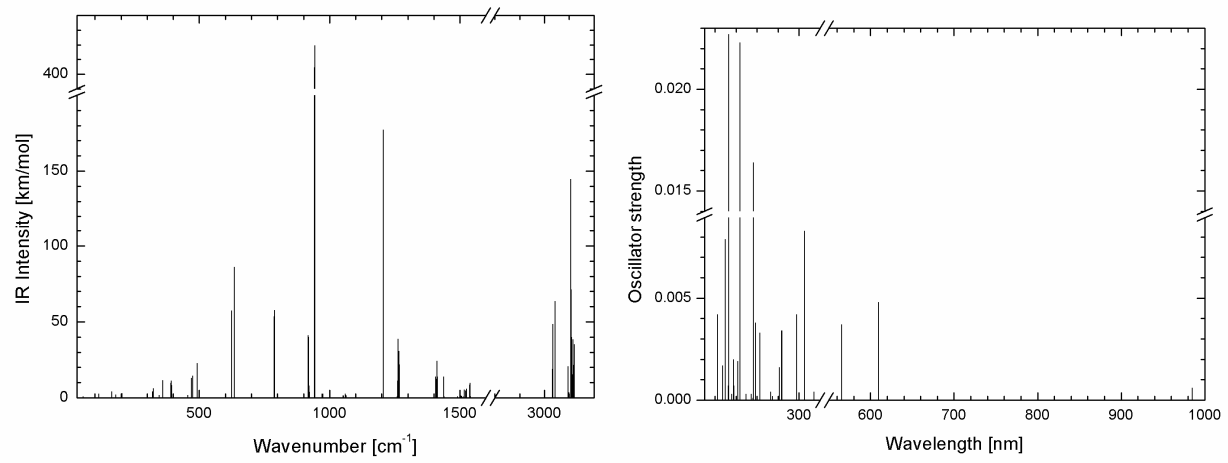

Figure S24. $^3[Cr(O^tBu)_4]^0 = {}^3[Cr(OCMe_3)_4]^0$

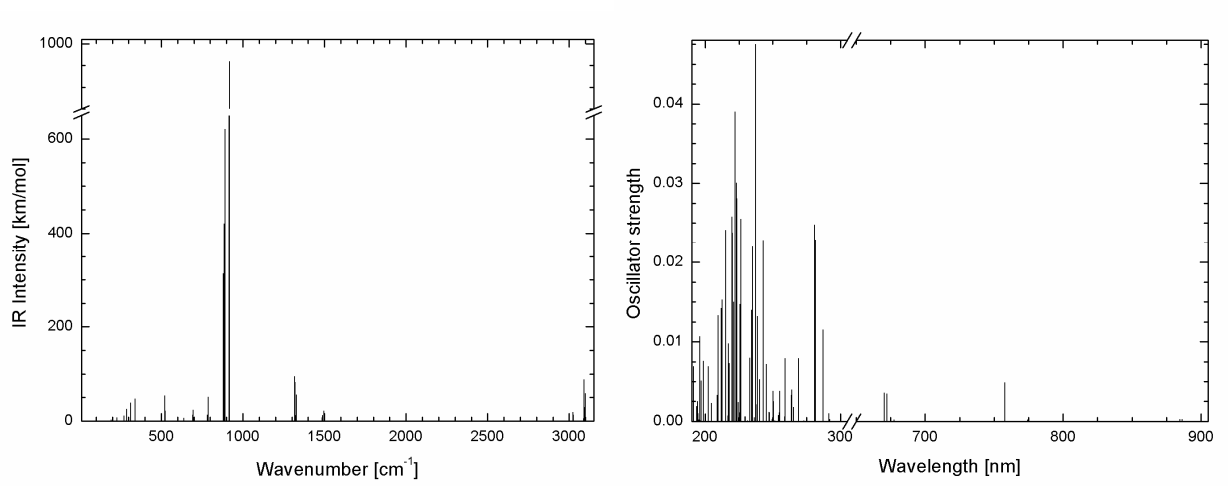

Figure S25. $^1[Cr(OSiMe_3)_4]^0$ (UB3LYP/6-311G*)

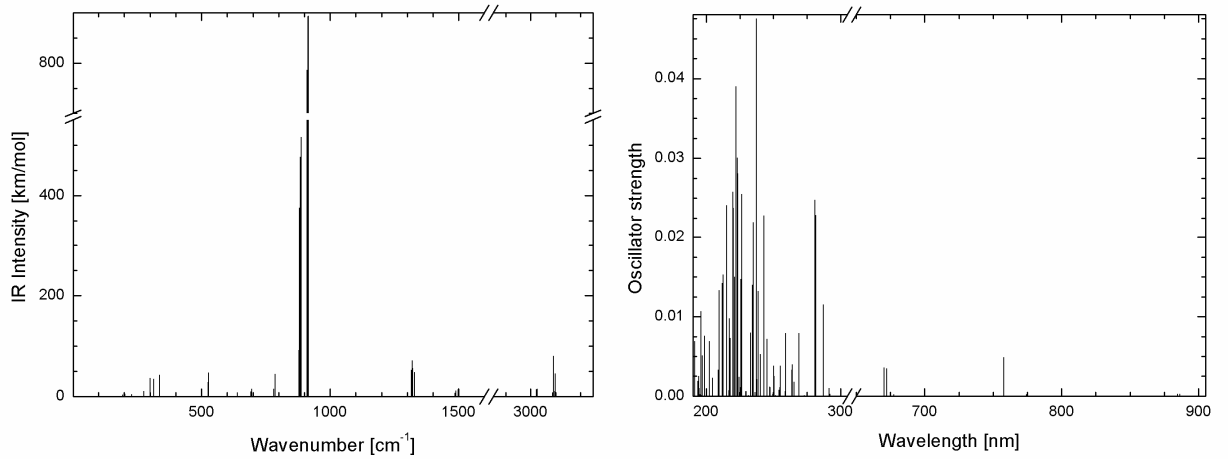

Figure S26. $^3[Cr(OSiMe_3)_4]^0$

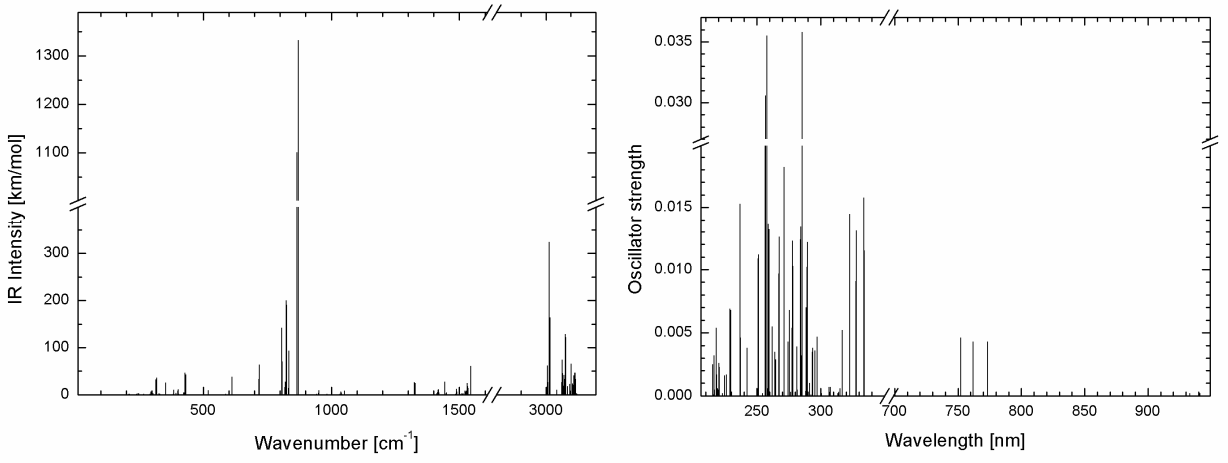

Figure S27. $^1[Cr(OSiMe^tBu_2)_4]^0$ = $^1[Cr(DTBMS)_4]^0$ (UB3LYP/6-311G*)

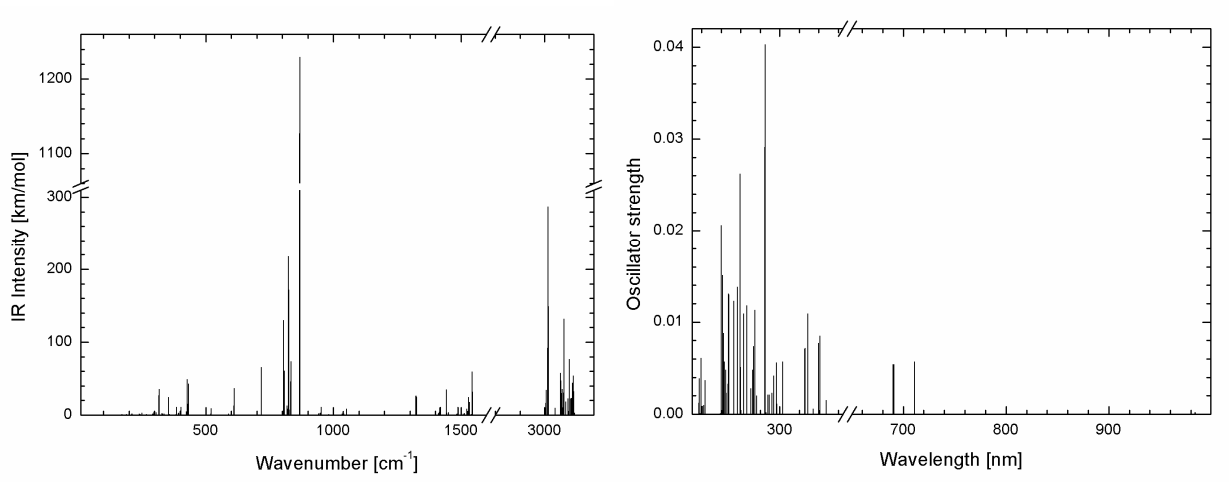

Figure S28. $^3[Cr(OSiMe^tBu_2)_4]^0$ = $^3[Cr(DTBMS)_4]^0$

References

1. Ward, G. A.; Bower, B. K.; Findlay, M.; Chien, J. C. W., Electron paramagnetic resonance of tetrakis(1-norbonyl)chromium. *Inorg. Chem.* **1974,** *13*, 614-617.
2. Mowat, W.; Shortland, A.; Yagupsky, G.; Hill, N. J.; Yagupsky, M.; Wilkinson, G., Elimination stabilized alkyls. Part I. Chromium, molybdenum, tungsten, and vanadium. *J. Chem. Soc., Dalton Trans.* **1972**, 533-542.
3. Mowat, W.; Shortland, A. J.; Hill, N. J.; Wilkinson, G., Elimination stabilized alkyls. Part II. Neopentyl and related alkyls of chromium(IV). *J. Chem. Soc., Dalton Trans.* **1973**, 770-778.
4. Ward, G. A.; Kruse, W.; Bower, B. K.; Chien, J. C. W., EPR spectra of chromium(IV) in tetrakis-alkyl chromium compounds. *J. Organomet. Chem.* **1972,** *42*, C43-C46.
5. Alonso, P. J.; Forniés, J.; García-Monforte, M. A.; Martín, A.; Menjón, B.; Rillo, C., Synthesis and characterization of new paramagnetic tetraaryl derivatives of chromium and molybdenum. *J. Organomet. Chem.* **2007,** *692*, 3236-3247.
6. Alonso, P. J.; Forniés, J.; García-Monforte, M. A.; Martín, A.; Menjón, B.; Rillo, C., A New Series of Homoleptic, Paramagnetic Organochromium Derivatives: Synthesis, Characterization, and Study of Their Magnetic Properties. *Chem. Eur. J.* **2002,** *8*, 4056–4065.
7. Alyea, E. C.; Basi, J. S.; Bradley, D. C.; Chisholm, M. H., Covalent compounds of quadrivalent transition metals. Part II. Chromium(IV) tertiary alkoxides and triethylsilyloxide. *J. Chem. Soc. A* **1971**, 772-776.
8. van Dam, P. J.; Klaassen, A. A. K.; Reijerse, E. J.; Hagen, W. R., Application of high frequency EPR to integer spin systems: Unusual behavior of the double-quantum line. *J. Magn. Reson.* **1998,** *130*, 140-144.
9. Wasserman, E.; Snyder, L. C.; Yager, W. A., ESR of the Triplet States of Randomly Oriented Molecules. *J. Chem. Phys.* **1964,** *41*, 1763-1772.
10. Weil, J. A.; Bolton, J. R., *Electron Paramagnetic Resonance: Elementary Theory and Practical Applications*. 2nd ed.; John Wiley & Sons, Inc.: Hoboken, NJ, 2007.
11. Basi, J. S.; Bradley, D. C.; Chisholm, M. H., Covalent compounds of quadrivalent transition metals. Part III. Chromium(IV) dialkylamides. *J. Chem. Soc. A* **1971**, 1433-1436.
12. Alonso, P. J.; Forniés, J.; García-Monforte, M. A.; Martín, A.; Menjón, B., The first structurally characterised homoleptic organovanadium(III) compound. *Chem. Commun.* **2001**, 2138-2139.
13. Alonso, P. J.; Forniés, J.; García-Monforte, M. A.; Martín, A.; Menjón, B., New Homoleptic Organometallic Derivatives of Vanadium(III) and Vanadium(IV): Synthesis, Characterization, and Study of Their Electrochemical Behaviour. *Chem. Eur. J.* **2005,** *11*, 4713-4724.
14. Marshak, M. P.; Nocera, D. G., Chromium(IV) Siloxide. *Inorg. Chem.* **2013,** *52*, 1173–1175.
15. Tregenna-Piggott, P. L. W.; Weihe, H.; Barra, A.-L., High-field, multifrequency EPR study of the $[Mn(OH_2)_6]^{3+}$ cation: influence of π-bonding on the ground state zero-field-splitting parameters. *Inorg. Chem.* **2003,** *42*, 8504-8508.
16. Tregenna-Piggott, P. L. W.; Spichiger, D.; Carver, G.; Frey, B.; Meier, R.; Weihe, H.; Cowan, J. A.; McIntyre, G. J.; Zahn, G.; Barra, A.-L., Structure and bonding of the vanadium(III) hexa-aqua cation. 1. Experimental characterization and ligand-field analysis. *Inorg. Chem.* **2004,** *43*, 8049-8060.
17. Van Stappen, C.; Maganas, D.; DeBeer, S.; Bill, E.; Neese, F., Investigations of the Magnetic and Spectroscopic Properties of V(III) and V(IV) Complexes. *Inorg. Chem.* **2018,** *57*, 6421-6438.

18. Abrahamson, H. B.; Brandenburg, K. L.; Lucero, B.; Martin, M. E.; Dennis, E., Spectroscopy and photochemistry of the tetranorbornyl complexes of titanium and chromium. *Organometallics* **1984,** *3*, 1379-1386.
19. Distortion from tetrahedral geometry and mixing of the states derived from ^{3}F and ^{3}P free-ion terms (as well as from singlet terms via spin-orbit coupling (SOC) and from ligand 2p AO contributions) make the other two potentially observable, along with possible spin-forbidden transitions.
20. Brorson, M.; Schäffer, C. E., Orthonormal interelectronic repulsion operators in the parametrical d^q model. Application of the model to gaseous ions. *Inorg. Chem.* **1988,** *27*, 2522-2530.
21. Ballhausen, C. J., *Introduction to Ligand Field Theory*. McGraw-Hill: New York, 1962.
22. Schäffer, C. E., A Perturbation Representation of Weak Covalent Bonding. *Struct. Bonding* **1968,** *5*, 68-95.
23. Bendix, J.; Brorson, M.; Schäffer, C. E., Accurate empirical spin orbit coupling parameters ζ_{nd} for gaseous nd^q transition metal ions. The parametrical multiplet term model. *Inorg. Chem.* **1993,** *32*, 2838-2849.
24. Bendix, J., Ligfield. In *Comprehensive Coordination Chemistry II, Volume 2: Fundamentals: Physical Methods, Theoretical Analysis, and Case Studies*, Lever, A. B. P., Ed. Elsevier: Amsterdam, 2003; Vol. 2, pp 673-676.
25. Chisholm, M. H.; Cotton, F. A.; Extine, M. W., Molecular and electronic structure of tetrakis(dimethylamido)molybdenum(IV). *Inorg. Chem.* **1978,** *17*, 1329-1332.
26. Reader, J.; Tauheed, A., Spectrum and energy levels of quadruply-ionized molybdenum (Mo V). *Journal of Physics B: Atomic, Molecular and Optical Physics* **2015,** *48*, 144001.
27. Ralchenko, Y.; Kramida, A. E.; Reader, J.; NIST ASD Team, NIST Atomic Spectra Database (ver. 5.5.6). National Institute of Standards and Technology: Gaithersburg, MD, 2018.
28. Use of B = 794 cm^{-1}, Dq = 943 cm^{-1} matches the two higher energy bands exactly, as reported by Alyea et al.,[7] but the lowest energy band is calculated 330 cm^{-1} too high.
29. Bochmann, M.; Wilkinson, G.; Young, G. B.; Hursthouse, M. B.; Malik, K. M. A., Synthesis and properties of bis(*t*-butyl)methoxides of chromium(III,IV), manganese(II), iron(III), cobalt(II), and copper(I). The crystal and molecular structures of lithium tetrakis[bis(t-butyl)methoxo]chromate(III)-tetrahydrofuran (1/1), tetrakis[bis(*t*-butyl)methoxo]chromium(IV), and lithium tetrakis[bis(*t*-butyl)methoxo]ferrate(III)-bis(*t*-butyl)-methanol (1/1). *J. Chem. Soc., Dalton Trans.* **1980**, 1863-1871.
30. Soriaga, R. A. D.; Nguyen, J. M.; Albright, T. A.; Hoffman, D. M., Diamagnetic Group 6 Tetrakis(di-*tert*-butylketimido)metal(IV) Complexes. *J. Am. Chem. Soc.* **2010,** *132*, 18014-18016.
31. von Wartenberg, H., Über höhere Chromfluoride (CrF_4, CrF_5 und CrO_2F_2). *Z. Anorg. Allg. Chem.* **1941,** *247*, 135-146.
32. Bougon, R.; Wilson, W. W.; Christe, K. O., Synthesis and characterization of tetrafluoroammonium hexafluorochromate and reaction chemistry of chromium pentafluoride. *Inorg. Chem.* **1985,** *24*, 2286-2292.
33. Prof. Dr. Sebastian Riedel, personal communication.
34. Jacobs, J.; Mueller, H. S. P.; Willner, H.; Jacob, E.; Bürger, H., Vibrational and electronic spectra of molecular chromium tetrafluoride, CrF_4, and chromium pentafluoride, CrF_5. Comments on the existence of chromium hexafluoride, CrF_6. *Inorg. Chem.* **1992,** *31*, 5357-5363.
35. See Figure 6a in Jacobs et al; also, Prof. Dr. Sebastian Riedel, personal communication.

36. McClure, D. S., Electronic Spectra of Molecules and Ions in Crystals. Part II. Spectra of Ions in Crystals. In *Solid State Physics*, Seitz, F.; Turnbull, D., Eds. Academic Press: New York, 1959; Vol. 9, pp 399-525.
37. Hedberg, L.; Hedberg, K.; Gard, G. L.; Udeaja, J. O., Molecular Structure of Chromium Tetrafluoride in the Gas Phase. *Acta Chem. Scand.* **1988,** *42a*, 318-323.
38. Stavropoulos, P.; Savage, P. D.; Tooze, R. P.; Wilkinson, G.; Hussain, B.; Motevalli, M.; Hursthouse, M. B., The synthesis and X-ray crystal structures of homoleptic tetrahedral aryls of osmium(IV) and of cyclohexyls of ruthenium(IV), osmium(IV), and chromium(IV). *J. Chem. Soc., Dalton Trans.* **1987**, 557-562.
39. Groysman, S.; Villagrán, D.; Nocera, D. G., Pseudotetrahedral d^0, d^1, and d^2 Metal−Oxo Cores within a Tris(alkoxide) Platform. *Inorg. Chem.* **2010,** *49*, 10759-10761.
40. Bader, R. F. W., *Atoms in Molecules: A Quantum Theory*. Clarendon Press: Oxford, UK, 1994.
41. Keith, T. A. *AIMAll*, 17.11.14; TK Gristmill Software: Overland Park, KS, 2017.
42. Schlöder, T.; Brosi, F.; Freyh, B. J.; Vent-Schmidt, T.; Riedel, S., New Evidence in an Old Case: The Question of Chromium Hexafluoride Reinvestigated. *Inorg. Chem.* **2014,** *53*, 5820-5829.